CHALMERS

High Power Motor Control Electronics for a Rear Axle Steer-By-Wire System

Master of Science Thesis in Embedded Electronic System Design

TOBIAS HALLBERG
JOEL OLOFSSON

Chalmers University of Technology
University of Gothenburg
Department of Computer Science and Engineering
Göteborg, Sweden, June 2015

High Power Motor Control Electronics
For a Rear Axle Steer-by-Wire

TOBIAS HALLBERG
JOEL OLOFSSON

Examiner: Per Larsson-Edefors

Chalmers University of Technology
University of Gothenburg
Department of Computer Science and Engineering
SE-412 96 Göteborg
Sweden
Telephone + 46 (0)31-772 1000

Department of Computer Science and Engineering
Göteborg, Sweden June 2015

Abstract

This thesis proposes and evaluates a solution for the power and control electronics needed for a rear-axle steer-by-wire system. The power electronics consists of transistors able to handle currents up to 400 A, gate drivers needed to drive these transistors, current measurement and heat sink design. The control electronics consists primarily of a microcontroller with protection on power supply and on peripherals attached.

In addition to this, two control algorithms for motor control were investigated, six-step commutation and field-oriented control. Six-step commutation scheme was mainly investigated in order to give the thesis workers, but also the reader, a reference tool in order to provide a better understanding of the more advance field-oriented control.

During the final test of the control electronics it was shown that the power electronics was indeed able to withstand the high currents flowing, but due to problems with the control electronics no control loop was tested.

Keywords: Steer by Wire, Rear Axle Steering, Field-Oriented Control, Motor control, Power Electronics

Preface

This Master's Thesis is carried out at CPAC Systems AB located in Mölndal, Sweden, during the spring semester of 2015. CPAC Systems AB is a part of the Volvo Group.

Acknowledgments

Firstly we would like to give a special thanks to our supervisor at CPAC Systems, Marcus Broberg for his support throughout the project. We would also like to thank Carl Björklund for general support, and Brian Bonafilia for his technical advice regarding motor control and hardware design. Finally we would like to thank Johan Angenete and Håkan Andersson for making this thesis work possible.

Tobias Hallberg, Joel Olofsson

Mölndal, June 17, 2015

Acronyms

AC	Alternating Current
ADC	Analog to Digital Conversion
ASIC	Application Specific Integrated Circuit
BOM	Bill Of Materials
BLDC	Brushless DC
CAN	Controller Area Network
DC	Direct Current
ECU	Electronic Control Unit
FPGA	Field-Programmable Gate Array
FR-4	Flame Resistant - 4
GPIO	General Purpose Input/Output
IGBT	Insulated-Gate Bipolar Transistor
JFET	Junction Field-Effect Transistor
MOSFET	Metal–Oxide–Semiconductor Field-Effect Transistor
PCB	Printed Circuit Board
PMSM	Permanent Magnet Synchronous Motor
RASBW	Rear Axle Steer-By-Wire
SBW	Steer-By-Wire
SPI	Serial Peripherals Interface

Contents

1 Introduction

CPAC Systems is currently investigating a concept for a Rear Axle Steer-By-Wire (RASBW) system. Systems like these remove the mechanical link between the steering wheel and the wheels that traditionally exist in all steering systems, making it possible to steer without any resistance. In order to provide the driver with feedback of the road's condition, which is present in the traditional mechanical systems, electronic devices are often implemented. These electronic devices can however limit the feedback and remove heavy forces and thus increase the driving comfort and relieve the driver from physical stress. Steer-by-wire systems also make it possible to increase the safety during extreme circumstances, when for example the vehicle is affected by external forces, by ensuring that the vehicle continues on the intended path in a way that could have been difficult to achieve for a driver [1]. Rear axle steering is used by heavy vehicles to improve maneuverability and reduce tire wear [2]. Adding an electronic control system the possibilities are extended even further. The current designs of steer-by-wire systems at the company only concern front axle steering, and they wish to extend this through an implementation of a steer-by-wire system for rear axle steering.

At present, CPAC Systems are planning to test a concept where an electric motor connected to a hydraulic system is used to control the steering of the rear axle of a heavy vehicle. The electric actuator will be used in combination with an already developed SBW system positioned on the front axle and, thus, relieve both axles from traditional mechanical steering. The rear axle steering actuator will be controlled by an electronic motor control system placed in the proximity of the rear axle. Releasing the rear-axle steering from the restraints of traditional mechanical steering will open up for new possibilities, such as significantly increased maneuverability of the vehicle in comparison with traditional rear axle steering.

1.1 Goal and Scope

The goal of the project is to specify and implement the electronic control system needed for the rear axle actuator in a prototype. This includes hardware design of an electronic motor control system based on a microcontroller, as well as evaluating different techniques for motor control.

The electronic motor control system consists of circuits for data bus communication, logic power supply, sensor interfaces and power electronics for controlling the actuators. Different techniques for motor control could consist of close-loop or open-loop control, using either a sensor or sensorless approach. A typical sensor based approach would use Hall-effect sensors to determine the current angle of the electrical motor, whereas a sensorless approach would measure the electromotive force (EMF) feedback from inactive coils.

The mechanical system which is to be controlled consists of a rear axle where the steering angle is adjusted by a hydraulic cylinder. The cylinder is in turn connected to an electric hydraulic pump, whose electric motor is to be controlled by the electric motor control unit.

To be able to withstand the expected usage environment, the prototype must fulfill certain requirements in terms of reliability. This entails meeting standards for temperature, voltage transients and mechanical stress as defined in standards such as AEC Q100 and Q101[3]. Since the application of the system can be considered to be safety critical, components certified for the functional safety standard ISO 26262 may be required [4].

In order for the system to be fully integrated, and be able to receive requested steering angles a communication bus is required. Communication will be conducted using the automotive standard bus Controller Area Network (CAN) [5]. Given the catastrophic events that can be caused by malfunction of the rear axle steering system, safety and reliability are the two most important requirements [6]. Any additional desired factor such as low energy consumption, small size and low manufacturing cost of the hardware are subordinate to the two main factors.

1.2 Limitations

This thesis work will be limited to developing software and hardware for an electronic motor control system, which includes control software, control electronics and power electronics. Parts of the resulting prototype will consist of mechanical parts, such as hydraulic pumps that will not be investigated as a part of this thesis work. Specifying and selecting the electric motor needed to interface the hydraulic pumps will also not be handled. This does not exclude an evaluation from the context of controllability of the provided electro-mechanical components.

1.3 Thesis Outline

First the required theory regarding electric motors, motor control algorithms and power electronics are described. This is followed by motivating and describing the chosen implementation. Then the results in terms of the electronic system are presented. Lastly the outcomes of these results are discussed and conclusions are drawn.

2 Technical Background

The rear axle steer by wire project will enable additional steering modes other than traditional steering, where the rear axle will act as a slave for the front axle steering. These steering modes could consist of for example a "crab" mode, where both the front and the rear axle are steering in the same direction making the vehicle move sideways. In Figure 2.1 the system is presented at a conceptual level. Where the subsystem marked with a thick black box is the focus of this thesis work. An

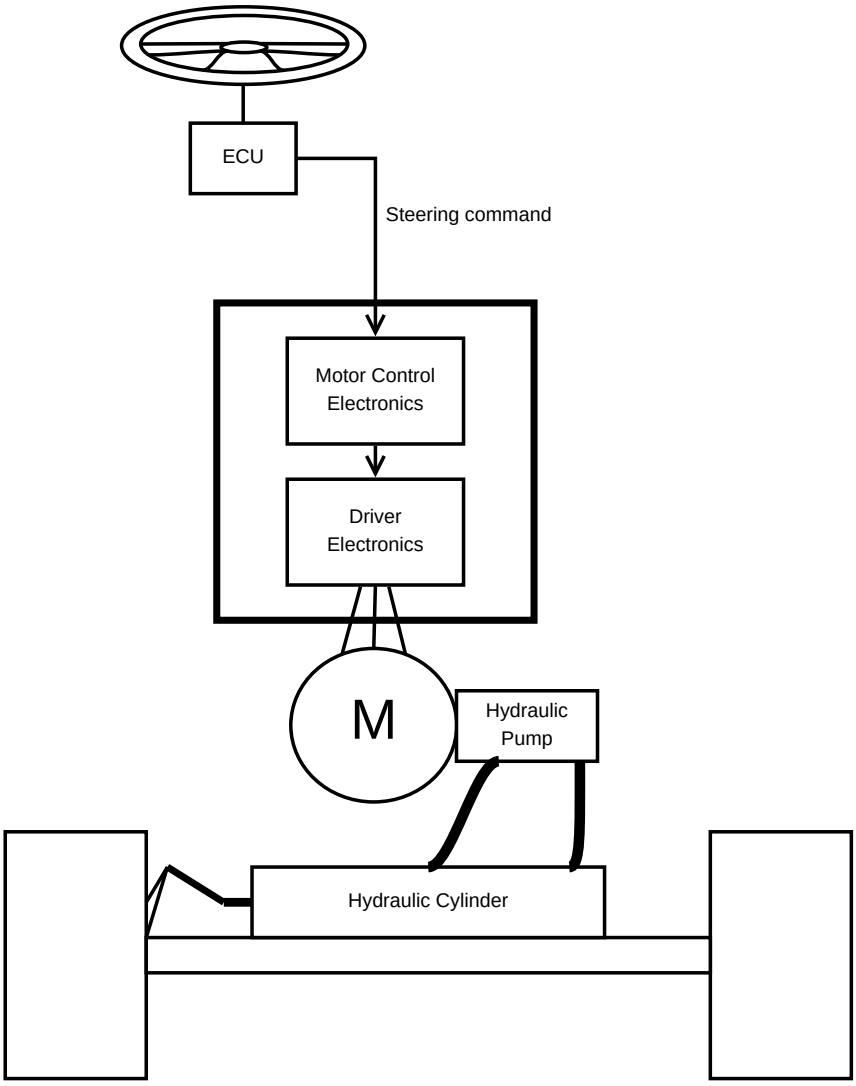

Figure 2.1: Overall system concept including the most important components.

electronic control unit or ECU will process driver inputs combined with the vehicles state to be able to send a correct steering command to the control system of the rear axle actuator. The steering command sent will be designed in a fashion that is not harmful to the vehicle or any person on board. It may however cause damage to the rear axle actuator unless preventive measures are taken. The damage that

may occur is characterized as an overload problem where components such as the electric motor or electric motor drive electronics can be overheated if the load is too high for an extended period.

The motor used in the system is a 3-phase permanent magnet synchronous motor (PMSM) which is a common type of brushless DC motor (BLDC). The motor is connected to a hydraulic pump which through a hydraulic cylinder is able to actuate steering of the rear axle. A built in position sensor of sine-cosine type is mounted in the motor, for rotor position sensing. In addition, a steering angle sensor is attached to the rear axle to provide feedback to the control system.

2.1 Electric Motor

An electrical motor is a machine that converts electrical energy to mechanical energy. Whereas there are several types of different motors, such as brushed and brushless DC motors and AC induction motors, they all consist of a stator and a rotor. The construction of the rotor and the stator does however differ between the different motor types and they all have their advantages and disadvantages. In this thesis report only the brushless DC motor (BLDC), and its subset the Permanent Magnet Synchronous Motor (PMSM) will be handled. The first commercially available electrical machines emerged in the late 1800s in the shape of the brushed DC motor. In the 1960s the BLDCs become commercially viable, this since the BLDC would need a more complex electronic control system, and therefore a need for control electronics. The advantage of a BLDC motor is higher efficiency and less need for maintenance since the construction is less susceptible to mechanical wear.

2.1.1 BLDC

The major difference between a brushless and a brushed DC motor is that in a brushed DC Motor the active coils are determined by the brush through the position of the rotor. In a BLDC motor however, the active coils needs to be determined in some other way. This is usually done with a position sensor or a sensorless approach by measuring the motors back electromotive force (EMF). Some form of control system is therefore required to activate different coils at correct moments of time.

The two fundamental components of a BLDC motor are the rotor and the stator. A description of these parts is given below, followed by an introduction to the voltage induced by these two components.

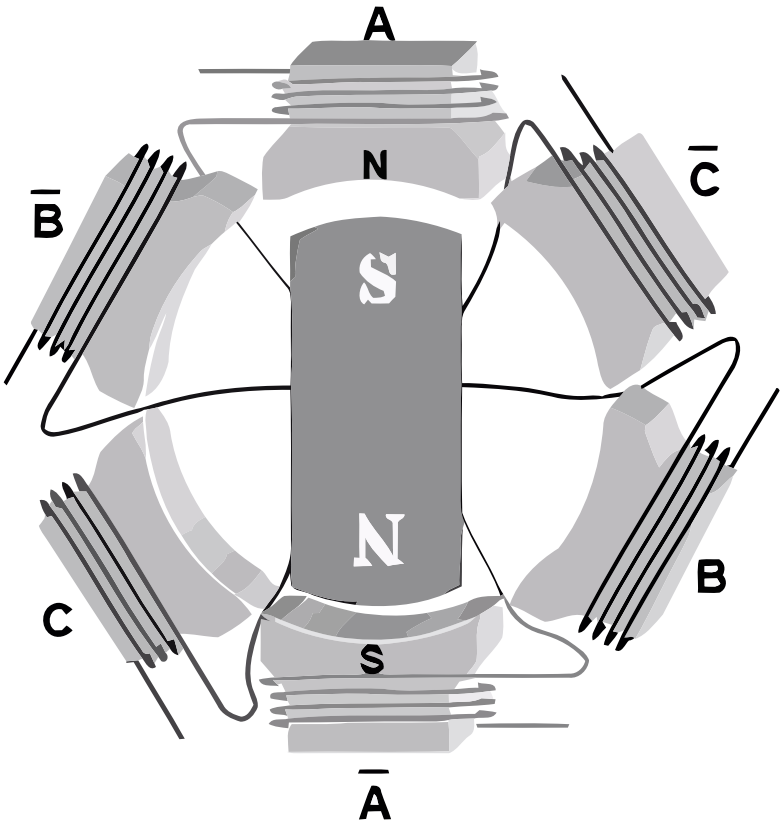

Figure 2.2: Simple illustration of a BLDC motor

Rotor

The moving part of a BLDC is called a rotor. The BLDC motor often has a rotor consisting of permanent magnets [7]. The rotor can have multiple pole pairs, where the number of pole pairs is defined as the number of south and north poles. The number of pole pairs determines a ratio between mechanical and electrical degrees, where one mechanical revolution (360 degrees) corresponds to $360 \cdot N_{pole-pairs}$ electrical degrees.

Stator

The stator holding the phase windings, are as the name implies, stationary with reference to the rotor. The stator in a BLDC must hold at least three phases, spread evenly with a distance of 120 degrees in order to eliminate deadlocks [1]. Through the windings, here on referred to as phases, current will flow producing a magnetic field, which will through repelling and attraction with the magnetic field of the permanent magnets in the rotor produce torque and eventually speed.

Back-EMF

Back electromotive force (back-EMF) is referred to as the voltage induced when the electric motor spins. As the permanent magnets of the rotor moves past the coils of the stator, in this sense making the electric motor a generator, the back-EMF will be induced in the opposite direction of the voltage applied to the stator phases. In an ideal electric motor, the generated back-EMF will be as high as the voltage applied to the motor[8]. The presence of back-EMF in combinations with certain motor parameters is useful for determining the position of the rotor without the use of any additional position sensor.

2.2 Power Electronics

The power electronics needed for driving a three-phase BLDC motor is based around the principle of pulling a phase either high or low. A schematic for such a driver can be seen in Figure 2.3. Two MOSFETs are connected to each of the phases in order to connect a phase to ground or supply voltage depending on the control signal given to the driver. To achieve this a minimum of 6 transistors is needed, the transistors act as switches and are usually of MOSFET or IGBT type, the need for 6 transistors is further described in Section 2.3.1. Using these transistors in combination with drive circuitry forms a unit called an inverter.

This chapter will give an introduction to the use of MOSFETs in power applications and compare them with IGBT devices.

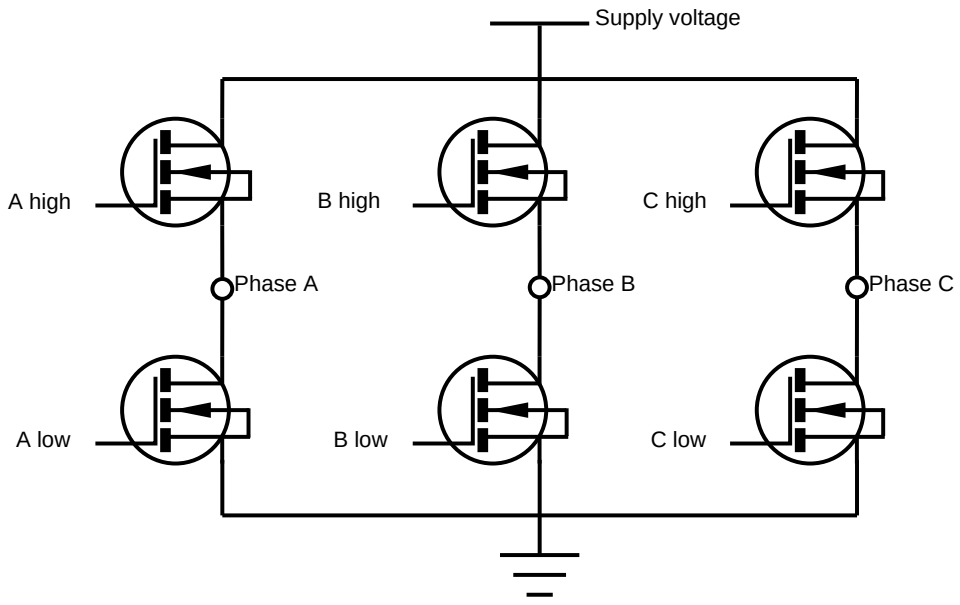

Figure 2.3: MOSFET based 3-phase motor driver.

2.2.1 Power MOSFETs

The processing techniques used to manufacture discrete power MOSFETs is very similar to the process used to manufacture the MOSFETs used in integrated circuits, even though the geometry is different and the voltage and current ratings are significantly higher [9].

Power MOSFETs are available with voltage ratings over 1000 V, and currents up to several hundred amperes. There is however a very important trade-off between these two parameters, which is caused by the physical properties of the MOSFET. One important property affecting this is the oxide thickness t_{ox} which is demonstrated in Figure 2.4 below. While a thin oxide layer is preferable to minimize the on-state resistance, a thicker layer is needed to achieve a higher breakdown voltage [9][10]. A more detailed discussion regarding the on-state resistance can be found in the section below.

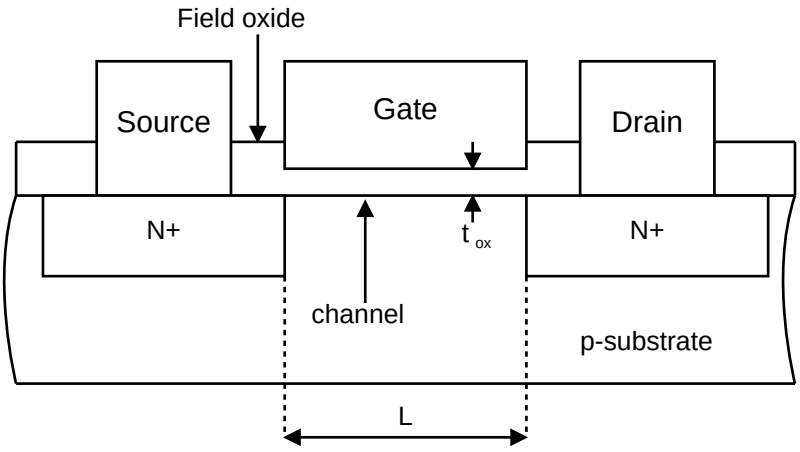

Figure 2.4: Internal structure of MOSFET

Effective on-state resistance $R_{DS(ON)}$

The on-state resistance $R_{DS(ON)}$ is one of the most important parameters to consider when selecting power MOSFETs for high currents since $R_{DS(ON)}$ has a great impact on the MOSFETs power dissipation. $R_{DS(ON)}$ depends naturally on the MOSFETs internal structure, seen in figure 2.4. It is given by equation 2.1 below:

$$R_{DS(ON)} = R_{source} + R_{channel} + R_{accumulation} + R_{drift} + R_{substrate} + R_{contact} \quad (2.1)$$

Where:

R_{source} is the source diffusion resistance

$R_{channel}$ is the channel resistance

$R_{accumulation}$ is the accumulation resistance

R_{drift} is the drift region resistance

$R_{substrate}$ is the substrate resistance

$R_{contact}$ is the sum of resistances in the bonding wires

The differences in the manufacturing process between devices for low and high voltage requirements are not only the thickness of the field oxide but also the resistivity of the wafer substrate [10, 9]. This is done to achieve a sufficiently high maximum V_{DS} [11].

A convenient property of MOSFETs is that $R_{DS(ON)}$ increases with rising temperature, which makes it possible to operate multiple power MOSFETs in parallel. The increasing on-state resistance during heating means that a MOSFET with higher a load than the ones that it is connected in parallel with will heat up more. The resistance will thus increase and will in turn decrease the current. In this way the MOSFETs will share the current and dissipate heat more evenly [9, 12].

Heat Dissipation Considerations

The most important difference between a signal MOSFET and a power MOSFET is that the latter is designed to withstand high currents along with the high heat that is generated when operating under high power conditions. This results in that the mayor difference between the two types of MOSFETs is that of the packaging-technique used. The package of the power MOSFETs needs to be able to transport the heat away from the MOSFET and to the package. When the heat has been transferred from the core to the package case the heat can then be [13]. There are also MOSFETs available which are designed to dissipate the generated heat into both the circuit board and an additional heat sink[14]. The different techniques and design considerations for distribution of heat are further discussed in section 2.2.3.

MOSFET Selection

When selecting a power MOSFET for a specific application there are several important parameters to consider. The most important ones being usually the on-state resistance $R_{ds(ON)}$ and the drain to source breakdown voltage V_{DS}. These two parameter create a trade-off, a MOSFET with a high forward voltage blocking capabilities will need to have thicker p-n junction and will thus have a higher $R_DS(ON)$ [10].

The on-state resistance will greatly affect the amount of heat dissipated by the power electronics circuit. The drain to source breakdown voltage must be set

significantly higher than the systems nominal voltage in order to withstand the transient voltages created by the system itself as well as other components in the electrical system [15]. Another important parameter is the gate charge Q_g, that will together with the desired switching rate give the required current that needs to be supplied by the gate drivers [16].

2.2.2 Power IGBTs

The Insulated Gate Bipolar Transistor can be said to functionality wise be a mix between the bipolar transistor and the MOSFET. It has the switching and conducting characteristics of a bipolar transistor but is voltage controlled like a MOSFET.

IGBTs have a negative temperature coefficient, which means that the resistance decreases as the temperature increases. While this might seem as a good property, it can potentially cause problems. While thermal runaway is the most obvious one, this property also makes it inappropriate to connect multiple IGBT in parallel since all current tends to flow through one transistor only [17].

2.2.3 Power Dissipation

The power dissipated from a power electronics circuit can have a large impact on the circuits physical implementation on a PCB. Maintaining the power dissipation at a controllable level is of high importance, since the lack of proper cooling considerations can not only limit the system's performance, but also lead to catastrophic failures in case of overheating. Therefore, considerations about the number of components and the size of the components both have its contributions and trade-offs, which will affect the PCB size and manufacturing cost.

Materials/Thermal Calculations

To be able to analyze heat transfer in a system, some tools are needed. In the case of electronic systems the concept of thermal resistance is often used. Thermal resistance is based upon Ohm's law to simplify heat transfer for persons that are more familiar with electronics than with thermodynamics. Thermal resistance is the reciprocal of thermal conductance which is shown for some common materials in table 2.1.

For low power applications the PCB alone with proper copper areas added can act as a heat sink. For applications with higher amounts of power a heat sink can be added on the opposite side of the PCB. To achieve the best thermal conductance, special techniques can be used when manufacturing the PCB. One option is Insulated Metal Substrate (IMS), where aluminum isolated with thin non conductive materials is used as the isolator in a circuit board. This process is more

seldom used and is more expensive than FR-4, which is the standard isolator used in PCB manufacturing.

Even though the material FR-4 has very poor thermal conductivity properties, it can still be used where good heat conducting properties are required. It does however mean that certain measures must be taken so that the heat can transfer through the board. A common and simple way is to add thermal vias, a thermal via has the same design as an ordinary via where the only difference is its purpose.

It is advantageous to fill the thermal vias with solder and thereby increase the effective area, this is however a disadvantage from a manufacturing point of view since additional steps have to be added to the manufacturing process. If filled vias are to be used the diameter must be kept small (0.3mm) to avoid solder from forming an uneven surface on the PCBs backside where the heat sink is to be attached.

To provide the best possible connection between the PCB and the heat sink, the solder mask on the PCB should be omitted on the heat transfer areas. An electrical isolator - called a thermal pad - with good thermal conduction properties are required in order to prevent short-circuits through the aluminum heatsink.

The most recent technology is a combination where MOSFETs can be cooled from heat sinks on both the bottom and top sides. This has the potential of reducing the needed board space [18]. As of this date the availability of these devices for prototype use is still very limited.

Table 2.1: Thermal and electrical properties for various materials.

Material	Thermal Conductivity $(W \cdot m^{-1} \cdot K^{-1})$	Thermal Capacity $(J/(g \cdot K)$	Electrical Resistivity $(28,2n\Omega m(at20C))$
Aluminium	180	0,91	28,2 nOhm m (at 20 C)
Copper	398	0,39	16.78 nOhm·m (at 20 C)
FR-4	0.2	-	
Steel	80.4	-	-
Solder	58	0,45	96.1 nOhm·m (at 20 C)

Design Considerations

The first design choice needed to be done is which MOSFETs and package to use. The choice of package will result in a difference throughout the design process as it will affect the possible cooling solutions for the transistors. The most common package types are:

- Through Hole
- Surface Mounted Device
- Surface Mounted Device with dual side cooling

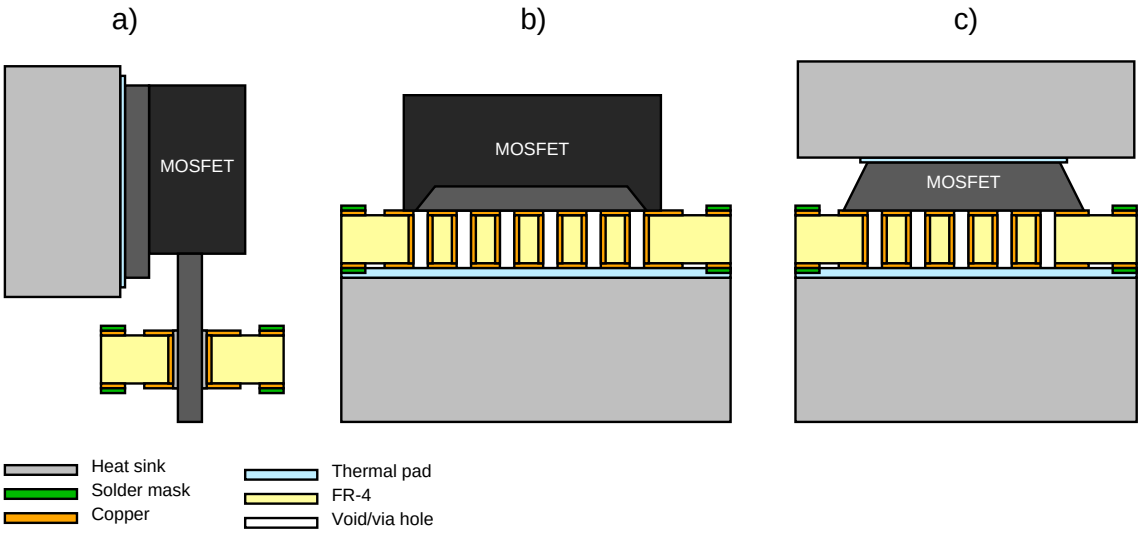

Figure 2.5: Three common principles for cooling power MOSFETs.

Heat Sink Designs

For circuits that generate significant amounts of heat, some form of cooling system is required. There are many solutions and depending on the given circumstances, only a few might be appropriate.

Cooling systems are usually divided into active and passive systems, where active means that the cooling system uses energy to transfer the heat away from its source. This usually involves moving mechanical parts, such as a fan, which have a negative impact on reliability and maintenance needs. Passive cooling systems on the other hand work by only absorb and more slowly radiate the heat to the ambient air. Both active and passive cooling systems are dependent on a heat sink to form a thermal connection with the heat source. There are several ways of attaching this heat source, where the most common ones are described below.

Since power MOSFETs are common heat sources in both this thesis project and in power electronics in general, it is used as an example. The classic approach is to use through hole mounted components according to Figure 2.5a, where the heat is kept away from the PCB and lead directly to the heat sink.

A more modern way is to use SMD components where usually one or several of the pads used for electrical connection is also used to distribute the heat away from the component, this can be seen in Figure 2.5b. For low to moderate amounts of heat this method can also be implemented without a dedicated heat sink, where extended copper surfaces on the board takes the role of dissipating the heat. This is a solution which is very attractive from a cost perspective.

Some MOSFETs that at the time being were just recently released to market is designed to be cooled from both the top and bottom in order to achieve the

best possible thermal properties. This leads to devices that can handle very high currents in relation to their PCB footprint size [18]. In Figure 2.5c a sketch of a cooling system for these MOSFETs is shown.

2.3 Controller Electronics

The purpose of an electronic control system is to control one or several actuators usually based on sensor readings. To perform this task some type of logic circuit is needed, this can be a microprocessor, a FPGA or an ASIC.

2.3.1 Motor Control

For every direction and magnitude of the created magnetic field, in reference to the rotors magnetic field, there is an optimal direction which will produce maximum torque, as well as a direction which will produce no torque. The optimal direction of the generated magnetic field (stator field) will occur when the difference between the stator field and the magnetic field of the rotor is at an angle of 90° electrically, whereas the direction that produces no torque will be when both the magnetic fields are aligned. In order to keep the motor spinning, the motor requires electric control of the stator field in order to keep the difference of 90° [19].

2.3.2 Pulse Width Modulation

Pulse Width Modulation (PWM) is a technique to modulate a signal into a square-wave with a fixed frequency, and a duty cycle proportional to the signal. For motor control applications the minimum PWM frequency is limited by the inductance of the motors windings. A motor with high inductance windings will thus perform well at a lower switching frequency, which is beneficial when dimensioning the MOSFET drivers [20].

2.3.3 Six-step Commutation

Six-step commutation is due to its simplicity and cost effectiveness a popular commutation method [21]. It typically uses three Hall-effect sensors placed with a distance of 120° around the electric motors stator for position sensing and six transistors to control the direction of current flowing through the stators of the electric motor. In six-step commutation, six different stator flux vectors are switched between, where in each step one high-side transistor and one low-side transistor are open [21]. This causes the current to flow in two of the phases at once, in positive direction for the phase with open high-side transistor and in negative direction for the phase with the

low-side transistor open. In Figure 2.6 a six-step commutation excitation scheme can be seen.

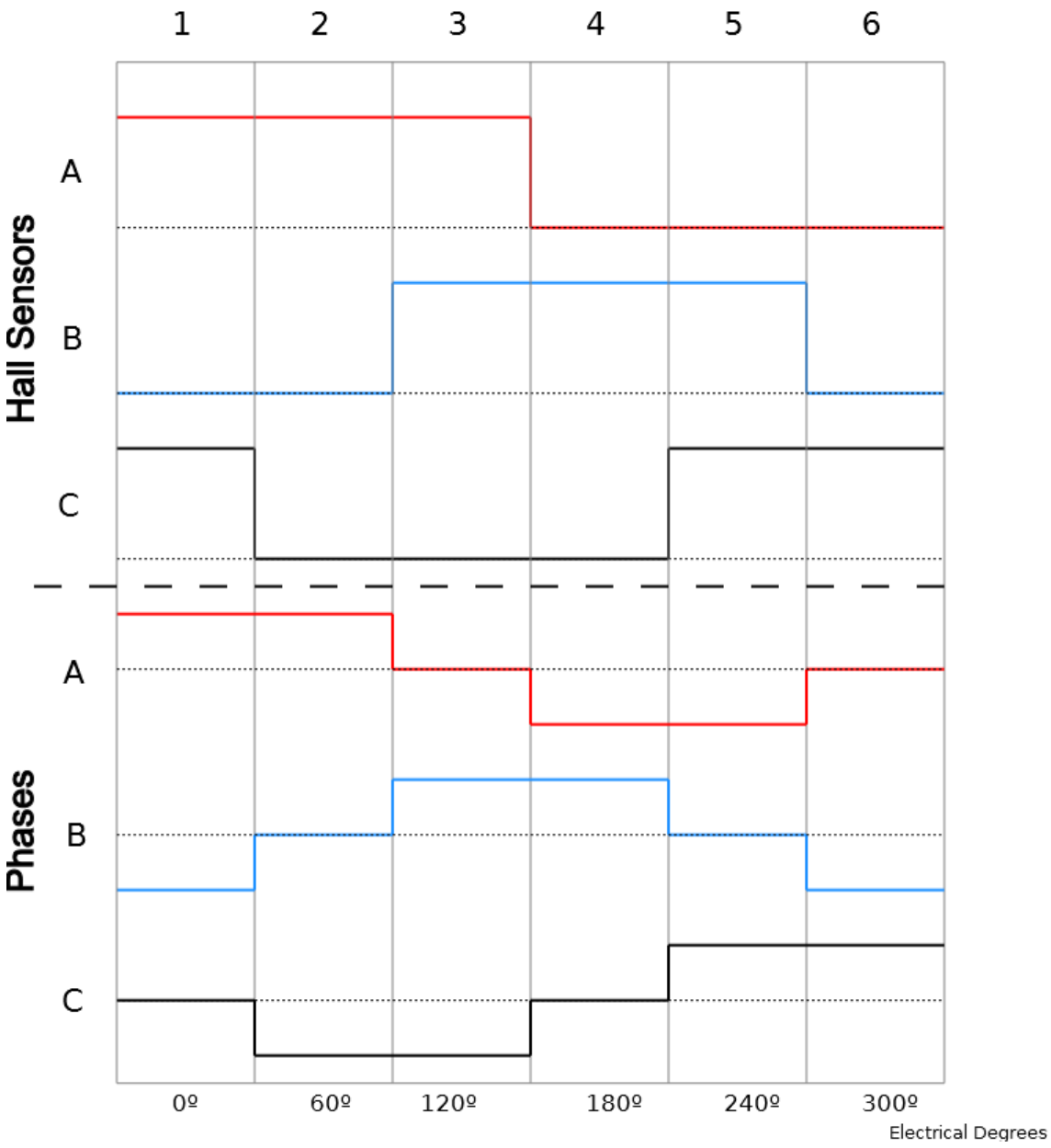

Figure 2.6: Six-step excitation scheme

In order to produce maximum torque, the angle between the stator and rotor fields should, as previously mentioned, be as close to 90° electrically as possible. When using this type of control scheme, the limitation of six stator field vectors, will not make it possible to keep the difference to 90°, instead the difference between stator and rotor fields will actually vary between 60° and 120° electrically causing ripple in the produced torque.

2.3.4 Field-Oriented Control

For systems with higher demands on dynamic performance, field-oriented control is often a more suitable solution. In field-oriented control, the stator current phases have been measured and transformed into a two dimensional stationary reference frame, called d-q frame. In the d-q reference frame the rotor flux is represented by the direct current i_d and torque by the quadrature current i_q.

The basic flow of implementing field-oriented control is to first measure the currents flowing in each of the stator phases. Then, using the Clarke and Park transform the measured currents are transformed into a 2-axis coordinate (α-β frame) system, first into a time varying coordinate system with the stator currents represented, then into a time invariant coordinate system (d-q frame) [19]. The transformation into a 2-axis time invariant coordinate system enables the use of more simplified control methods, since we are now actually controlling DC. The currents are then, using the inverse form of the Clarke and Park transform, back into time-varying coordinate system and uses Space Vector Modulation (SVM) to calculate the PWM signals to generate the magnetic field. SVM is further described in this section.

Clarke/Park Transform

In order to simplify the analysis of a three phase system we want to transform the three time-varying stator currents into a 2-axis time invariant coordinate system. This is done through the Clarke and Park transform. The first step is the Clarke transform, which will transform the three phase system into a two-phase stationary orthogonal coordinate system. In other words, the three phases placed evenly with a angle of 120° now has been transformed into two vectors with a 90° angle. The transform is conducted as seen in Equation 2.2

$$\begin{bmatrix} i_\alpha \\ i_\beta \end{bmatrix} = \begin{bmatrix} \frac{2}{3} & -\frac{1}{3} & -\frac{1}{3} \\ 0 & \frac{1}{\sqrt{3}} & -\frac{1}{\sqrt{3}} \end{bmatrix} \begin{bmatrix} i_a(t) \\ i_b(t) \\ i_c(t) \end{bmatrix} \tag{2.2}$$

In order to remove the dependency of rotor a Park transform is typically done. This will move the currents into a reference frame that is synchronous with the rotor field.

$$\begin{bmatrix} i_q \\ i_d \end{bmatrix} = \begin{bmatrix} \cos\theta & \sin\theta \\ -\sin\theta & \cos\theta \end{bmatrix} \begin{bmatrix} i_{alpha} \\ i_{beta} \end{bmatrix} \tag{2.3}$$

where θ is the rotor position.

The stator currents are now transformed into a orthogonal rotating frame where i_d is directly aligned with the rotor field, and the current i_q which is in quadrature with the rotor field, this means that in order to have the torque-producing vector i_q at an angle of 90° with respect to the rotor field we would want to keep the direct current i_d as close to zero as possible. This since the motor itself already has a permanent magnet, in other words all the needed magnetic flux to keep the motor spinning is already produced by the motor itself.

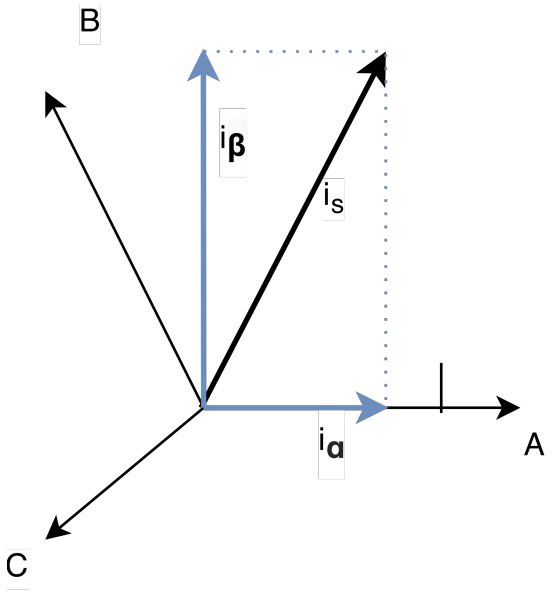

Figure 2.7: Reconstruction using Clarke transform

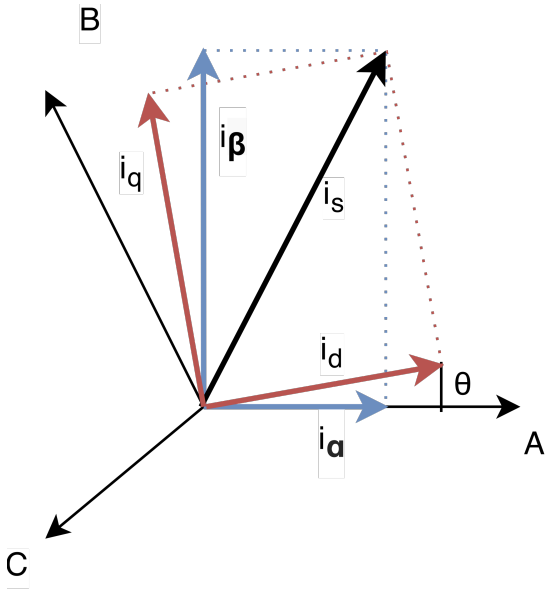

Figure 2.8: Reconstruction using Park transform

Space vector modulation

Space vector modulation is a control scheme using PWM [22]. The space vector modulation scheme treats the inverter as a single unit, rather than each of the three phases alone. Space vector modulation is designed in a way that enables the possibility to produce any voltage vector possible, thus making it possible to always produce a field orthogonal to the field of the rotor. Since we now are controlling the inverter as a single unit, we have 6 switches that each can take two states, on and off. This gives us $6^2 = 36$ possible states. However, most of the states could actually end

up damaging the hardware used, for example when a high side transistor and a low side transistor on the same phase are open at the same time. Therefore, the space vector modulation will only be able to take six different states, plus two additional states called the null states (one where all the high side transistors are on, and one where all the low side are on). The different combinations of high and low switches with corresponding states can be seen in Figure 2.9.

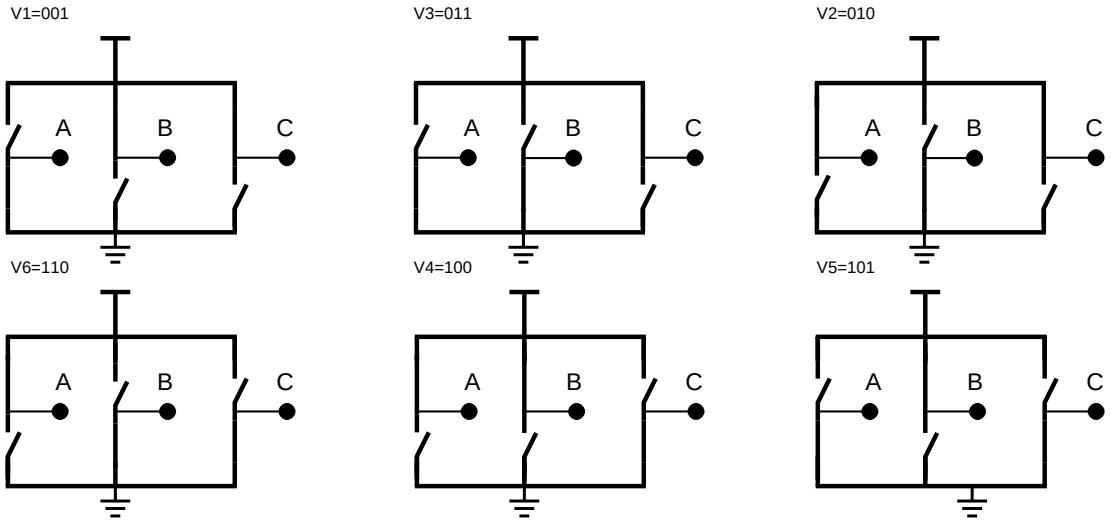

Figure 2.9: Basic six space vectors

The final step of the field-oriented control and the space vector modulation is to calculate the PWM duty cycles to be applied. This is done by projecting the desired/calculated vector reference vector as seen in Figure 2.10. The most usual way of determining the sector is by using the α and β vectors, that have been acquired through the inverse Clark transform[23]. Since the field-oriented control only uses 8 states in order to create a voltage reference, the control loop will have to alternate between several of these states. This is done once the sector has been determined, then the two adjacent Space Vectors and one of the aforementioned null vectors will be modulated between at a time T_0, T_1 and T_2, in order to create the reference vector V_{ref} as seen in Equation 2.4.

$$V_{ref} = T_2 \cdot V_3 + T_1 \cdot V_1 + T_0 \cdot V_{null} \tag{2.4}$$

Where T_0, T_1 and T_2 are ratios for duty cycle for the respective space vectors.

Waveforms

In Figures 2.11, 2.12 and 2.13 the theoretical voltages and currents generated by the field-oriented control algorithm, and the transformation from AC to DC can clearly be seen. In Figure 2.11 the voltage output calculated using space vector modulation can be seen.

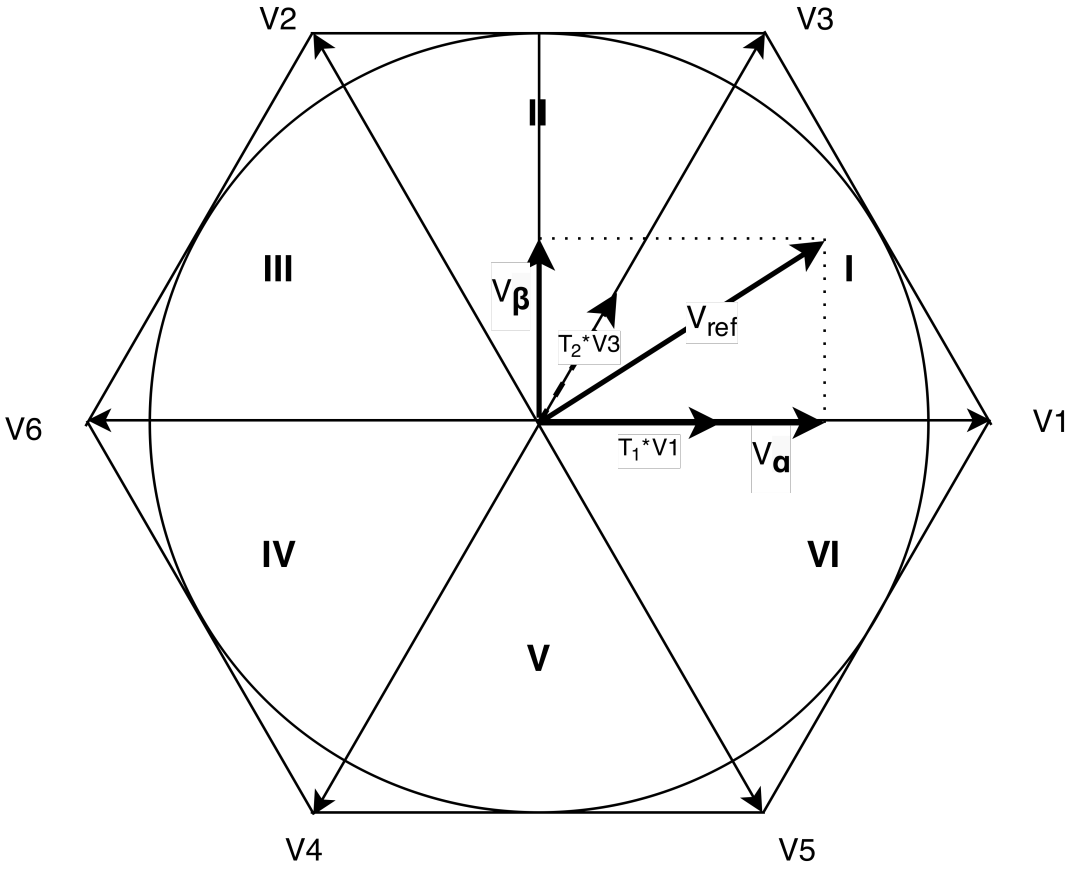

Figure 2.10: The six different states used in space vector modulation

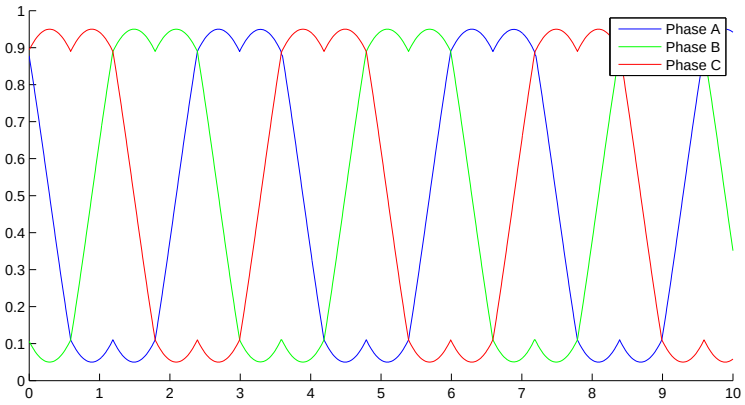

Figure 2.11: Voltage levels for the three phases

Figure 2.12 shows the Clarke transformed phase alternating currents.

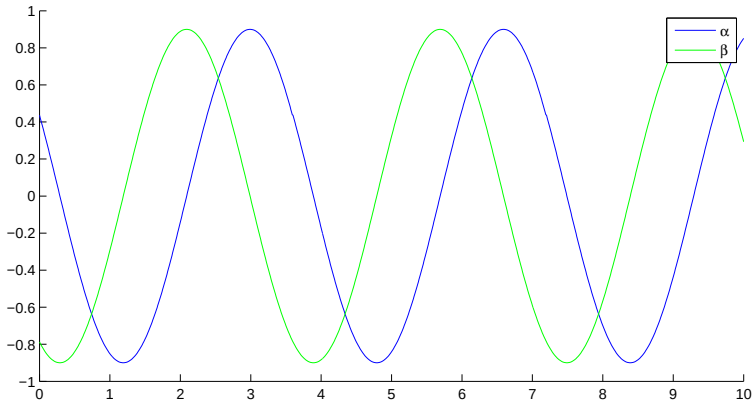

Figure 2.12: α and β currents resulting from Clarke transform

Lastly Figure 2.13 shows the currents transformed to direct current using Park transform.

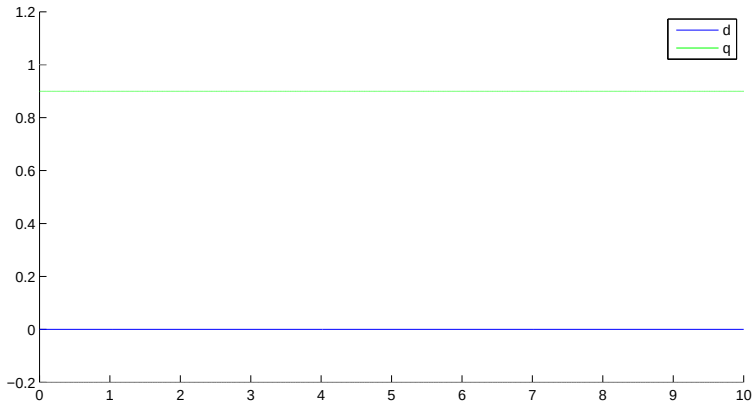

Figure 2.13: d and q currents resulting from park transform

Field-Weakening

As the rotation speed of the electric motor increases, so does the generated back-emf. At a certain point, defined as the base speed, the back-emf voltage would surpass the voltage of the inverter driving the motor. As a consequence the inverter would no longer be able to increase the speed further by producing more torque. And as stated in Section 2.3.4 the direct current i_d is directly aligned with the rotor field. This could be used to weaken the flux generated by the permanent magnet in the rotor, and consequently lower the back-emf allowing the inverter to further increase the speed. In order to achieve this, the rotor flux could be weakened by applying a negative direct current i_d [24].

2.3.5 CAN Communication

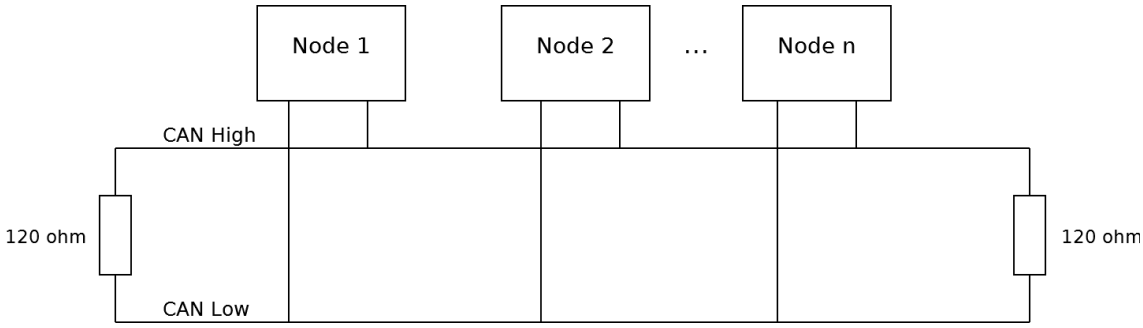

Figure 2.14: Example of CAN bus

Controller Area Network (CAN) is a communication standard used in automotive as well as industrial applications. CAN differ from most other communication protocols since the nodes on a CAN-bus do not have individual addresses. Figure 2.14 shows the principle of a single CAN-bus with n nodes. All nodes are connected to the same pair of wires and two 120 Ω termination resistors are placed at the end of the wires. The resistors serve as pull-down resistors and to minimize reflection [25].

The two wires are called CAN high and CAN low, and are measured differentially. To achieve higher noise rejection the wires are arranged as a twisted pair [26].

The information which is sent on the bus consist of maximum 8 bytes and is identified by the message id. The id tells the nodes which type of data that is carried by the CAN message. A lower message id will guarantee a higher message priority through bit-wise arbitration. The bit-wise arbitration works through recessive and dominant bits, logic 1 is recessive and logic 0 is thus dominant. During the arbitration sequence all nodes that wish to send a message on the bus will output their id simultaneously, starting with the least/most significant bit of the message id. For each bit the state of the bus is also measured, so that if a node is outputting a recessive bit but finds a dominant bit on the bus, the node will know that another message with higher priority is about to be sent, and will thus stop the transmission and wait for a new opportunity to transmit [26, 25].

Since there are no node addresses, a message sent on a CAN-bus will reach all nodes attached to the bus. A node receiving a message can, depending on its role in the system, either use or dismiss the received data. The message id is used for contention-resolution during data transmission [27, 25].

Message Frames

A node connected to the CAN bus can chose to send four different types of message frames [25]:

- **Data Frame** - Most common frame, containing data for transmission
- **Remote Frame** - Frame used for requesting data
- **Overload Frame** - Used to input delay between multiple data frames or between data frame and remote frame
- **Error Frame** Frame sent by any node on the bus detecting an error

The data frame can in more detail be divided into five fields [25]:

- **Arbitration** - The arbitration field holds the identifier of the message that is to be sent
- **Control** - In the control field the number of bytes that is to be sent is given (0-8 bytes)
- **Data** Field containing data to be sent
- **Cyclic redundancy check** Checksum sent in order to detect erroneous frames
- **End of Frame** Field containing recessive bits to indicate end of frame

3 Implementation

The implementation follows three different tracks and will guide the reader through the design choices made, as well as some calculations necessary for correct dimensioning of various components. These three tracks consist of the design of the driver board, followed by the design of the controller board and finally the field-oriented control is discussed.

3.1 Driver Board

The driver board was designed to control a specific motor used in a specific application. The motor model is ME1114 and the specifications are listed in Table 3.2 found on page 39 [28].

Since the currents through the motor windings are directly proportional to the applied torque, average and maximum current values could be determined to act as minimum requirements for the driver boards current handling capability. It was therefore determined that the driver board needed to withstand 150 A of current continuously and 400 A momentarily. The final design of the driver board can be seen in Figure 3.1

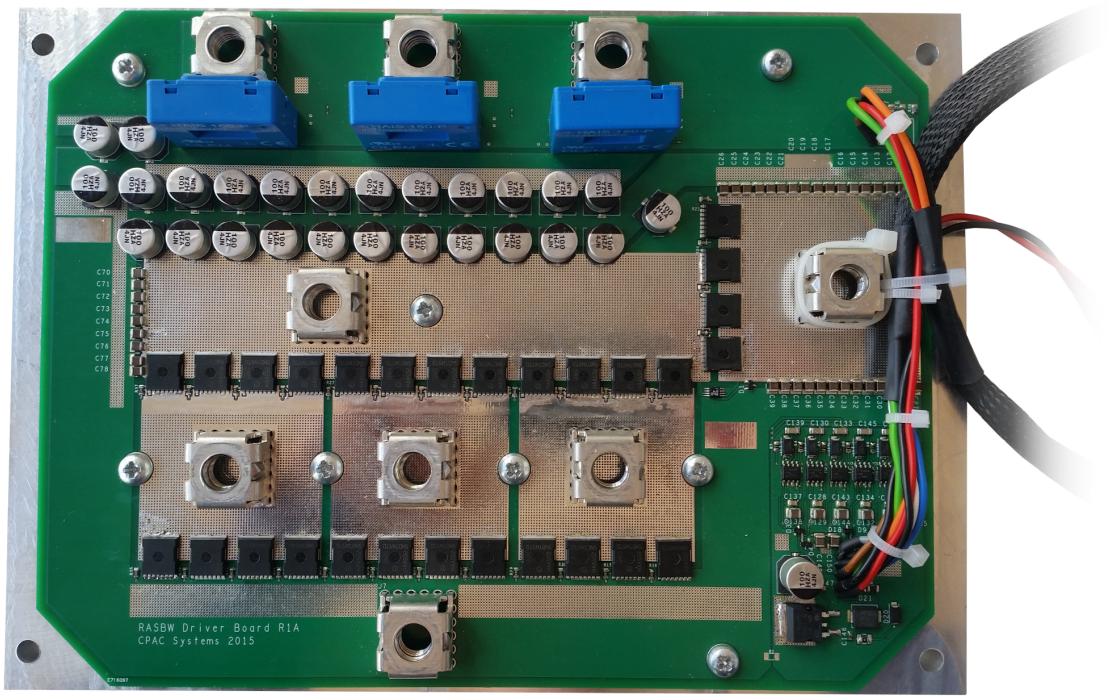

Figure 3.1: Photograph of the final driver board

3.1.1 Voltage Regulation

The gate drivers implemented in this design requires a 15 V input. Due to space limitations of the driver board the voltage regulation proposed in Section 3.2.2 is not a feasible option. Instead a linear voltage regulator is implemented. One of the major drawbacks discussed in that section is the heat dissipation of the voltage regulator, this will however not pose any problems for this implementation, since the circuit board in general is designed to handle a lot of heat. Also, the loss of efficiency using a linear voltage regulator can in the context of an inverter of this size be considered negligible.

For this application a 78-series linear voltage regulator, along with protection circuitry against transients and other present voltage spikes was used. For protection a transient-voltage-suppression (TVS) diode was implemented for protection against transients, and a varistor was placed to handle voltage abnormalities present for a longer duration of time. The circuitry and voltage regulator implemented for the driver card can be seen in Figure 3.2.

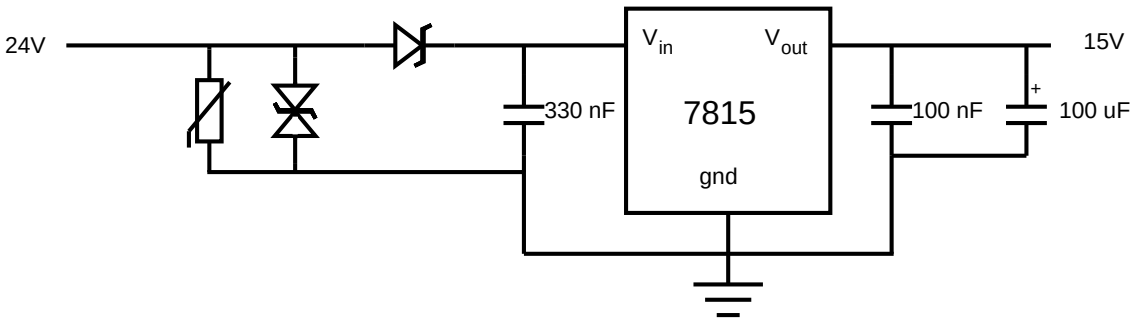

Figure 3.2: Schematic view of voltage regulator on the driver board

3.1.2 MOSFET Dimensioning and Selection

The requirements for the inverter is an operating voltage of 24 V and a peak current of 400 A.

V_{DS} for the power MOSFETs must be significantly higher than the battery voltage due to transients, loads dumps and back-EMF caused by the inductance in the motor. In order to meet the high requirements several MOSFETs can be connected in parallel to distribute the current as well as minimizing the dissipated power. Figure 3.3 shows how much heat that will be dissipated in total and in each MOSFET relative to the number of MOSFETs used in each low/high-side drive stage. Two MOSFETs were chosen to demonstrate how a difference in on-state resistance will affect the power dissipation of the inverter for between 1 to 10 MOSFETs connected in parallel.

The IPT015N10N5 MOSFET which is represented by the two left plots have

a R_{DS} of 1.5 m Ω while the IPT007N06N represented to the right

has R_{DS} = 0.75 m Ω[29] [30]. The power dissipation curves were plotted assuming a peak current of 400 A.

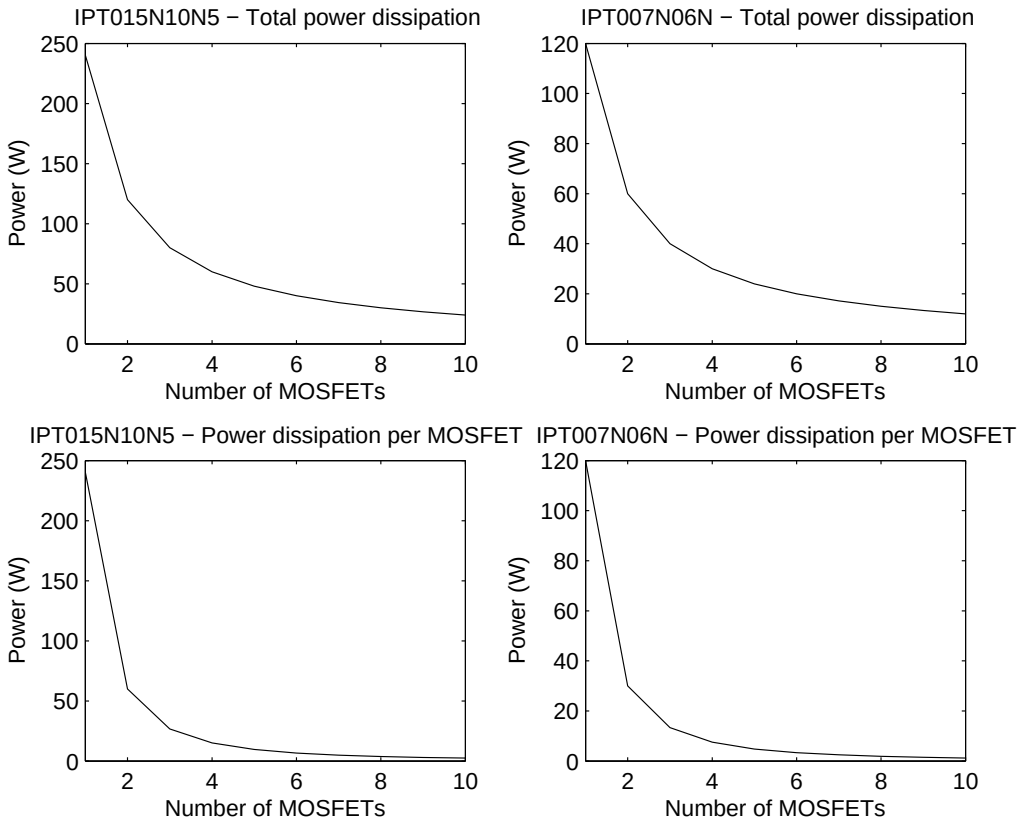

Figure 3.3: Comparison of heat generated using the IPT015N10N5 and IPT007N06N power MOSFETs from International Rectifier.

As can be seen in figure 3.3 the IPT015N10N5 is the preferred MOSFET option over IPT007N06N. The amount of dissipated power is approximately 50% less for the IPT007N06N MOSFET than for the IPT015N10N5 one. This means that a lower number of MOSFETs needs to be connected in parallel if choosing the IPT007N06N.

To provide the best possible connection between the PCB and the heat sink, the solder mask on the PCB should be omitted on the heat transfer areas. An electrical isolator - called a thermal pad - with good thermal conductions properties is required in order to prevent short-circuits through the heat sink.

The most recent technology is a combination where MOSFETs can be cooled from heat sinks on both the bottom and top sides. This has the potential of reducing the needed board space [18]. As of this date the availability of these devices for prototype use is still very limited.

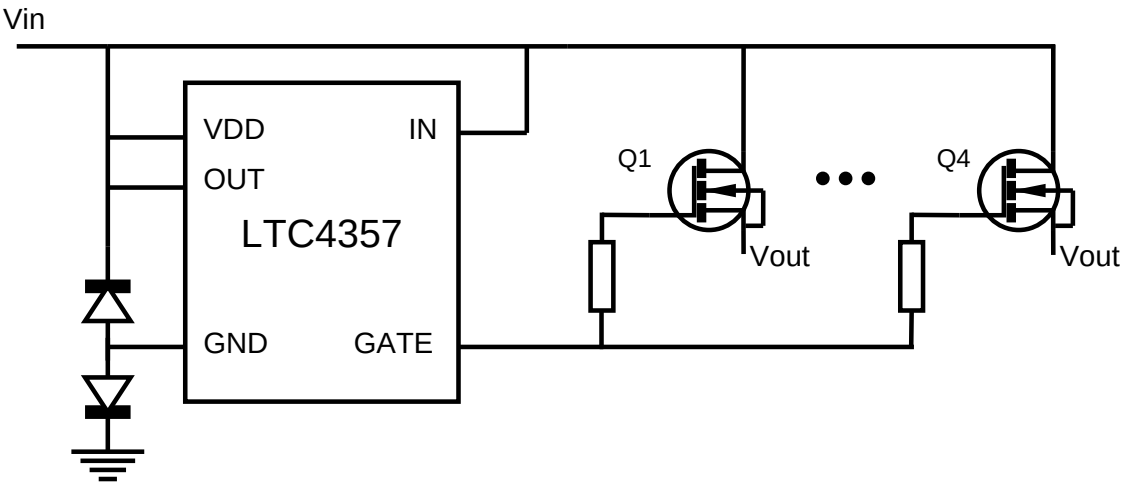

Figure 3.4: Schematic view of the LTC4357.

Considering this information it was decided to use 4 IPT007N06N MOSFETs connected in parallel, this results in a power dissipation of 7.5 W per MOSFET. The IPT007N06N comes in a SMD package which needs cooling on the bottom side of the PCB.

3.1.3 Polarity Protection

In this system polarity protection circuitry on the input to the source of the high side transistors have been implemented. Due to the high currents flowing in this system, the same design considerations regarding power dissipation as presented in Section 3.1.2 was taken. This resulted in use of the LTC4357 ideal diode controller, along with four of the IPT007N06N transistors [31, 30]. In Figure 3.4 a schematic view of the polarity protection circuitry can be seen.

3.1.4 Gate Drivers

The powerful MOSFETs and IGBTs used to drive large currents have high input capacitances C_{gs}. To be able to drive the gates of these devices from a microcontroller, a gate driver needs to be connected in between the two components. The gate driver accepts logic level signals as input and will in turn drive the gate with much higher currents and voltages than an MCU can provide.

As discussed in section 3.1.2, in order to handle the heat dissipation of 400 A of maximum current running through the motor 4 MOSFETs are implemented in parallel on each side and phase. The main requirement of the gate driver that needs to be taken into account is the peak drive current. This current is based on how quickly the transistors need to be opened for the particular application and is

calculated as seen in Equation 3.1 [32]:

$$dT = \frac{dV \cdot C}{I} \tag{3.1}$$

where:

dT = turn-on/turn-off time

dV = gate voltage

C = gate capacitance

I = peak drive current

and by using the relationship $Q_g = C \cdot V$ the peak drive current can now be calculated as seen in Equation 3.2

$$I = \frac{Q_g}{dT} \tag{3.2}$$

For this application a typical switching frequency of 20kHz will be considered. It is also assumed that the rise time of no longer than 0.4% of the PWM period is acceptable. Using the IPT007N06N transistors with a maximum gate charge of $Q_g = 211$ nC the peak drive current for each of the MOSFETs is then calculated as seen in Equation 3.3 and 3.4

$$dT = \frac{1}{20kHz} \cdot 0.4\% = 200ns \tag{3.3}$$

$$I = \frac{211nC}{200ns} = 1.055A \tag{3.4}$$

With these figures in mind, the FAN7190 with a current driving capability of 4.5 A from Fairchild Semiconductors was deemed as a suitable gate driver [33]. In order for the design to be future-safe it was also decided to use two drivers for each phase, thus limiting the driving current to 2.11 A per gate driver.

To be able to drive a N-channel MOSFET placed on the high side, a voltage V_{req} higher than the sum of the threshold voltage V_{th} and the source voltage V_s is needed. So a voltage of $V_{req} > V_{th} + V_{sys}$ is at least required.

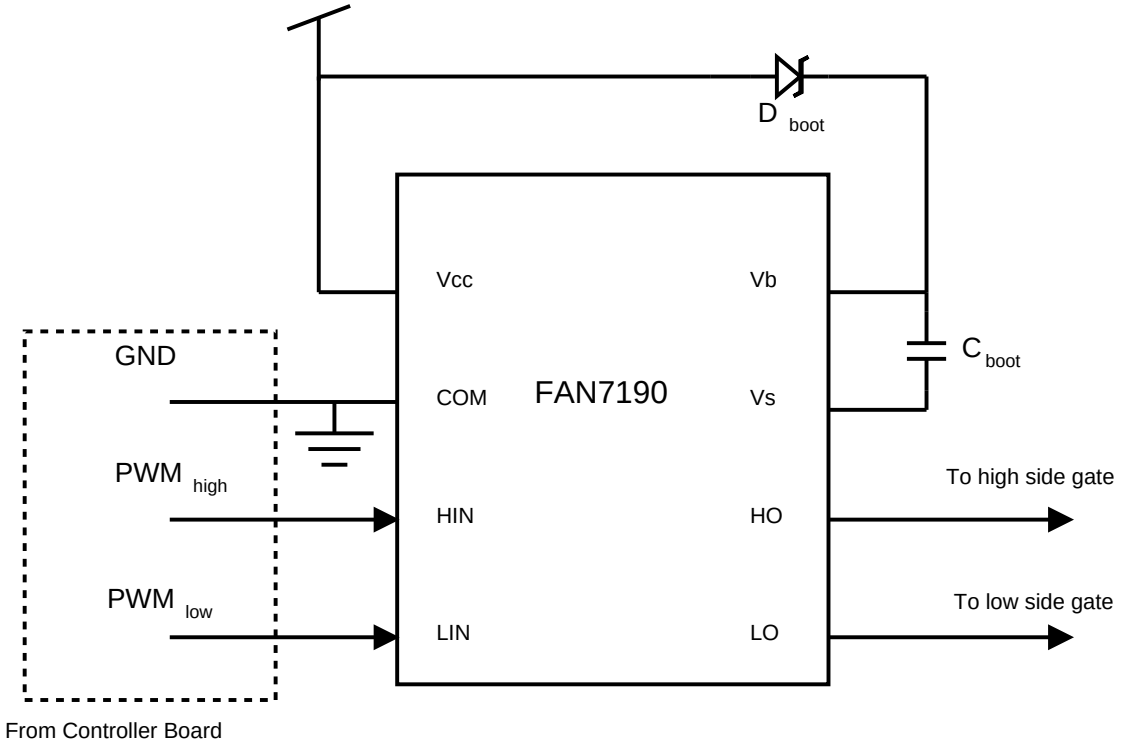

Figure 3.5: Schematic view of the gate driver

3.1.5 Bootstrap Capacitor

As mentioned in the previous section, in order to make the MOSFET fully conduct, an even higher voltage is needed. There are several established methods for generating this voltage. The most commonly used technique for this is bootstrap capacitors which are dimensioned as seen in Equation 3.5 [34].

$$C_{boot} = \frac{Q_{total}}{\Delta V_{boot}} \tag{3.5}$$

where $\Delta V_{boot} = V_{dd} - V_{DForward} - V_{GSMIN}$ and ΔV_{boot} is the maximum allowable voltage drop on the bootstrap capacitor.

$$Q_{total} = Q_{GATE} + I_{LKGS} + (I_{LKCAP} + I_{QBS} + I_{LK} + I_{LKDIODE}) \cdot t_{ON} + Q_{LS} \tag{3.6}$$

where:

Q_{GATE} = Total gate charge

I_{LKGS} = Switch gate-source leakage current

I_{LKCAP} = Bootstrap capacitor leakage current

I_{QBS} = Bootstrap circuit quiescent current

I_{LK} = Bootstrap circuit leakage current

Q_{LS} = Charge required by the internal level shifter

T_{ON} = High-side switch on time

$I_{LKDIODE}$ = Switch gate-source leakage current

For the Schottky rectifier D_{boot} the 10MQ100NPbf with a forward voltage drop of 0.85 V was selected, resulting in a ΔV_{boot} that could be calculated as follows. [35]. Assuming that $V_{GSMIN} = 5$V, which would correspond to a maximum current drain I_D of 400 A. With these parameters the ΔV_{boot} now can be calculated to be 15 V$-$0.85V$-$5 V$=$ 9.15 V. It was also decided to use ceramic capacitors as bootstrap capacitors, this since the leakage current of ceramic capacitors is so low that it can be neglected. For this calculation the high-side on time was assumed to be 50% of the PWM period of 20 kHz, the following list gives the parameters used for calculating Q_{total} and the result can be seen in Equation 3.7.

Q_{GATE} = 211 nC

I_{LKGS} = 100 nA

I_{LKCAP} = 0

I_{QBS} = 110 μA

I_{LK} = 50 μA

Q_{LS} = 3 nC

T_{ON} = 25 μs

$I_{LKDIODE}$ = 1 mA

$$Q_{total} = 211nC + (100nA + 0 + 110\mu A + 50\mu A + 1mA) \cdot 25\mu s + 3nC \rightarrow Q_{total} = 243nC \tag{3.7}$$

In order to keep the voltage drop as small as possible the Q_{boot} should be several (15-20) times greater than Q_{total}, resulting in a bootstrap capacitance of [36]:

$$\frac{Q_{total} \cdot 20}{9.15V} = 531nF \tag{3.8}$$

Using the e12-series a 560 nF capacitor was then selected.

3.1.6 Power dissipation

This section will go through all the precautions made starting with the MOSFET package and moving through all necessary layers for transferring heat and allowing for maximum power dissipation in the MOSFETs.

MOSFETs

The MOSFETs selected, the IPT007N06N from Infineon comes in a surface mounted package called PG-HSOF[30]. The PG-HSOF resembles a lot the d^2pak package, but have lower thermal resistance in junction-to-case [37]. The PG-HSOF package limits the cooling possibilities to only one feasible option, to place the bottom layer of the PCB on a heat sink and transfer the heat through the PCB.

Heat sink

Since the exact load profile of the motor driver is unknown, but assumed to be highly intermittent, a passive cooling solution with very high thermal capacity was considered appropriate. The theory is that the large amounts of heat generated during the load peaks will be absorbed by the heat sink and then slowly dissipated to its surroundings.

The heat sink used was milled out of a block of aluminum, with clearance holes for through hole components as well as for components mounted of the back side of the PCB. This resulted in a heat sink with a mass of approximately 2.2 kg.

A CAD-model of the heat sink can be seen in Figure 3.6. A thermal pad has been placed on the heat sink in order to provide galvanic isolation between the PCB and the heat sink. The thermal pad allows heat to transfer relatively well while a dielectric surface is maintained.

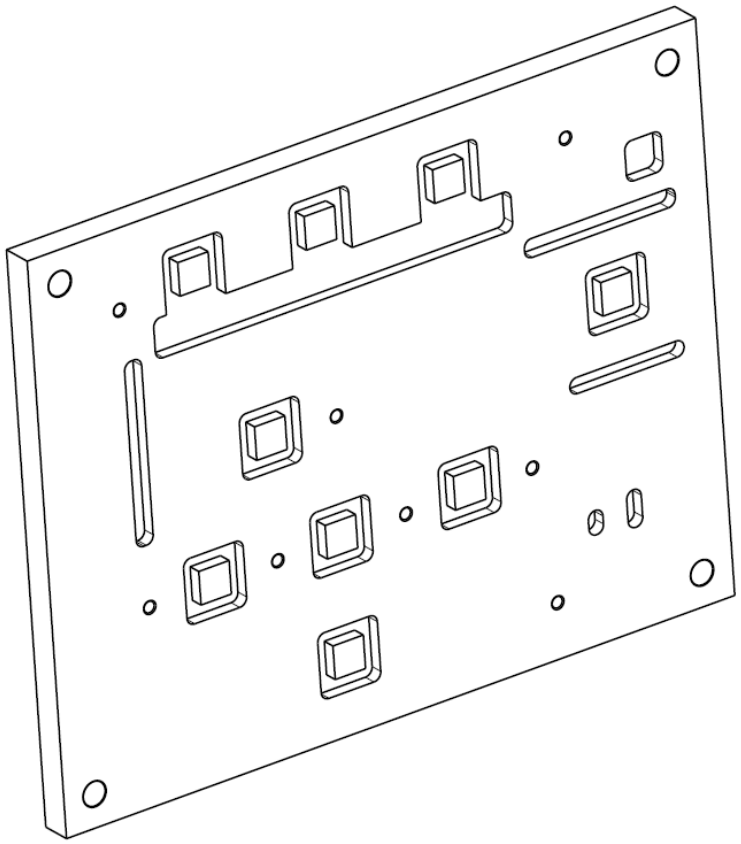

Figure 3.6: CAD model of the heat sink designed

In addition to the thermal capacity of the heat sink, the heat sink is to be mounted on a rig made of steel. This will further increase the effective thermal capacity by having the rig act as an extension of the heat sink.

PCB

The decision to base the design of the inverter upon a standard 2-layer PCB with 70 μ m thick copper was made. The reason for this is the current and heat conducting abilities in relation to the cost of manufacturing. Whereas both the size and performance could be improved by using a multi-layer board with thicker copper layers, the chosen option was deemed suitable for a prototype.

The PCB was designed with large copper areas in regions that were to become subject to high currents, namely the power and ground connections, and each of the motors three phases. On these large copper areas, the solder mask of the circuit board was removed on the most critical areas to create a direct contact with the thermal pad on the heat sink, as well as exposing the top surface of the PCB directly to air, thus enabling for increased heat transfer.

Since the heat sink and power MOSFETs are placed on the opposite sides of the PCB, thermal vias were added to minimize the thermal resistance between the two. As previously discussed in Section 2.2.3, FR-4 has very high thermal resistance. The copper plating inside the thermal vias will thus greatly reduce the thermal resistance between the two layers of the board on the applied areas.

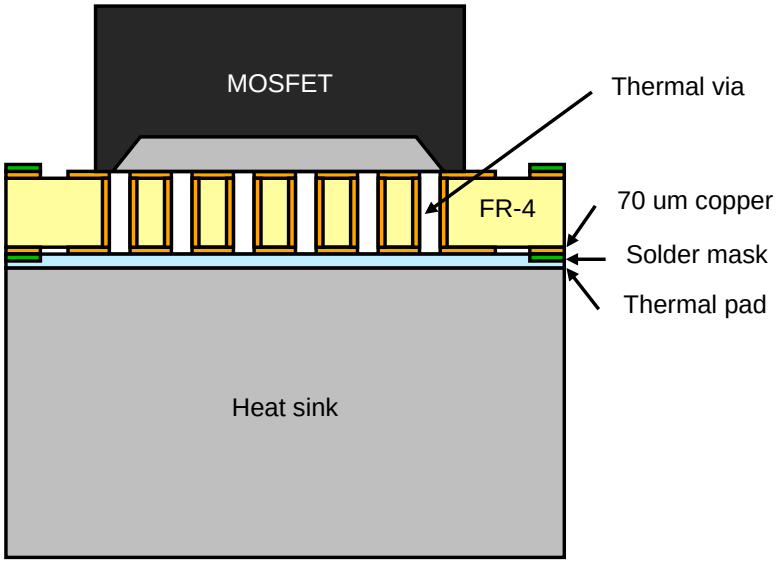

Figure 3.7: Heat transfer path from heat source to heat sink.

Calculations

In order to verify our design, calculations in this section were used. As previously described, the thermal circuit for the MOSFETs consists of a copper layer without a solder mask on both the top and bottom layers, thermal vias, a dielectric thermal pad and then screwed unto a heat sink. The total thermal resistivity can be summed as seen in Equation 3.9.

$$\theta_{junction-to-case} + \theta_{copper-top} + \theta_{via} + \theta_{coppper-bottom} + \theta_{thermal-pad} + \theta_{heat-sink} \quad (3.9)$$

Using Equation 3.10 and the data from Table 3.1 on page 31 and table 2.1 found on page 10 we can calculate the total thermal resistance as seen in Equations 3.11 through 3.14 with the junction-to-case resistance 0.2 W/K of the MOSFET used

$$\theta = \frac{I}{k \cdot A}. \quad (3.10)$$

where:

I is the thickness of the material

k is the thermal conductivity of the material

A is the area

Table 3.1: Characteristics for the different features used to distribute heat

Via Height	1.6 mm
No Vias/pad	140
Via Diameter	0.3 mm
PCB Thickness	1.6 mm
MOSFET Pad Area	80.8 mm^2
Copper Thickness	70 μm
Thermal Pad Thickness	0.2 mm
Heat Sink Thickness	12 mm

$$\theta_{vias} = \frac{1.6mm^2}{140 \cdot 58 \cdot \pi \cdot \frac{0.3}{2}^2} = 2.788°C/W \tag{3.11}$$

$$\theta_{copper} = \frac{70\mu m}{398 \cdot 80.8mm^2} = 0.002°C/W \tag{3.12}$$

$$\theta_{thermal-pad} = \frac{0.2}{0.8 \cdot 80.8mm^2} = 3.094°C/W \tag{3.13}$$

$$\theta_{heat-sink} = \frac{12mm}{180 \cdot 80.8mm^2} = 0.825°C/W \tag{3.14}$$

Since all the layers are in series the total thermal resistance is summed to get a total resistance of $\theta_{total} = 6.911$°C/W. If the ambient temperature of the heat sink is considered to be 21°C and using the IPT007N06N transistor with a maximum operating temperature of 175°C the maximum amount of power that can be dissipated in each of the MOSFETs can be calculated as seen in Equation 3.15.

$$P_{max} = \frac{T_{max} - T_{ambient}}{\theta_{total}} = \frac{175°C - 21°C}{6.911°C/W} = \frac{154°C}{6.911°C/W} = 22.28W \tag{3.15}$$

This offers much higher power dissipation for each MOSFET than the 7.5 W that was discussed in Section 3.1.2.

3.2 Controller Board

In order for an electronic control unit to function reliably in an automotive environment, some aspects of the design needs special attention. To be able to survive in a harsh automotive environment, an ECU must among other things be able to withstand and be protected against load dumps, voltage transients and reverse polarity supply voltage.

The Automotive Electronics Council (AEC) is an organization that has defined a set of standards for qualifying electronic components for use within vehicles. It is preferable to select parts approved according to the AEC standards when designing automotive electronics [3]. Since the end application must fulfill ISO26262, which is a safety standard for road vehicles, measures is taken to ensure future compatibility

with the standard. ISO26262 states 4 different safety grades, ASIL (Automotive Safety Integrity Level), ranging from A-D where ASIL D is the highest safety grade [4].

In this section the specification and special considerations that have been made for the design of the controller board are discussed. For this application, the controller boards is the PCB where all control electronics, such as Microcontroller Unit (MCU) and sensor interfaces have been placed.

The specification and lowest number of peripherals needed to be supported by the controller board can be seen in the following list, and the final manufactured PCB with mounted components can be seen in Figure 3.8

- 6 PWM channels
- 6 ADCs
- 1.25 V, 3.3 V and 5 V logic power supply
- 2 CAN-buses

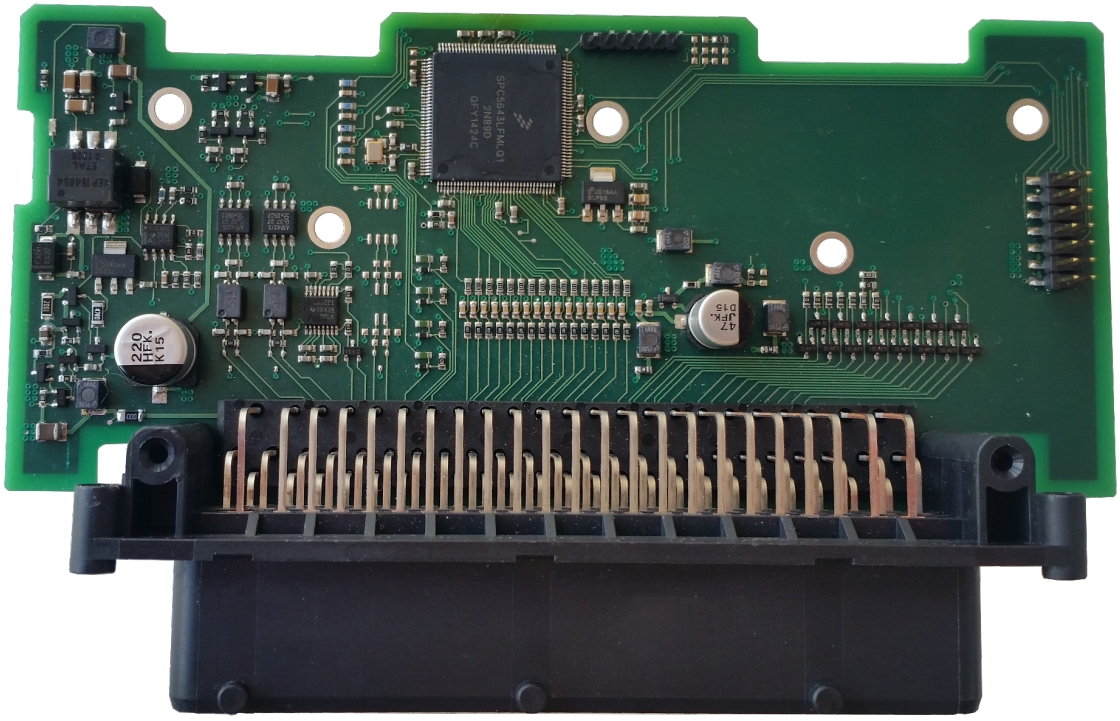

Figure 3.8: Photograph of the final controller board

3.2.1 Microcontroller

For interfacing with sensors and executing control software, the MPC5643L microcontroller from Freescale was chosen [38]. The MPC5643L is based on a 32-bit

PowerPC dual-core architecture, with the possibility of running one of the cores in lockstep mode for fail-safe operation. It has a maximum clock frequency of 120 MHz. The processor was chosen due to ASIL D and automotive certifications, as well as full support for the Motor Control Toolbox for MATLAB/Simulink further described in Section 3.3.2. ASIL D certification is critical since the processor in the end application must fulfill the ISO26262 standard [4]. Additionally, the microcontroller has all the necessary peripherals for communication, such as CAN and SPI, and sufficient number of ADC channels and PWM modules needed for this application.

3.2.2 Voltage Regulation

The MPC5643L implemented in this project requires 1.25 V, 3.3 V for logic levels and 5.0 V. In order for this controller board to be compliant with automotive standards for power supply's, it must accept input voltages in the range of 6-36 V. In order to supply voltage with this wide input range, circuitry for voltage regulation was implemented. For this application a switched-mode DC-to-DC converter deemed suitable and was implemented for the 5.0V supply. The use of a switching converter allows for higher efficiency and less heat dissipation than for going with a linear voltage regulator, but suffers from a more complex design. In this project, the converter was implemented using the PWM control circuit TL5001 from Texas Instruments with a power FET attached to the voltage output [39]. The feedback resistance seen in Figure 3.9 for the TL5001 was calculated as $V_{out} = 1 + \frac{R_1}{R_2} \rightarrow 5V = 1 + \frac{R_1}{R_2}$ which gives us a ratio of four between the feedback resistors R_1 and R_2. The data sheet for the TL5001 specifies that the input load to the feedback should be at least 100kΩ, therefore a value of 200kΩ was chosen for $R1$ and 50kΩ for R_2. Due to the high switching noise from the transformer, this was placed as far as possible from the logical signals.

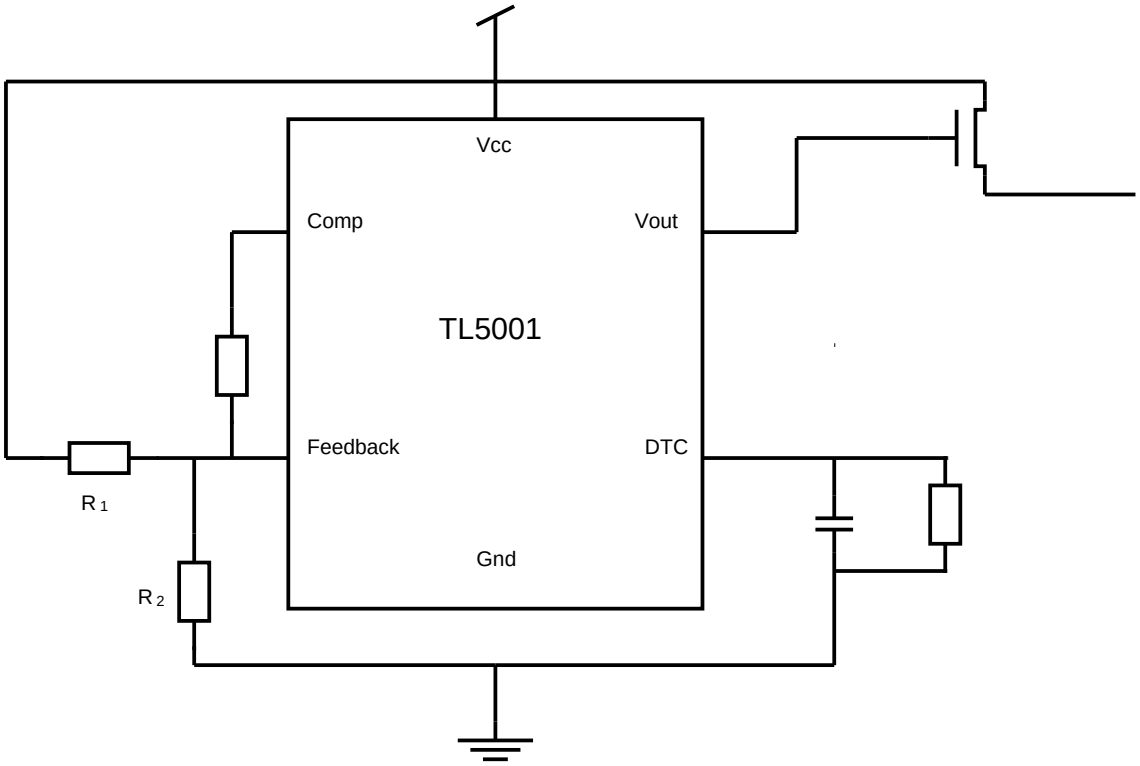

Figure 3.9: Schematic view of the DC-to-DC transformer

For the 3.3 V supply a linear voltage regulator was implemented, and the 1.25 V is regulated by the MCU using an external transistor [38].

Additionally, since the end-application for the controller board is within the automotive industry, the controller board must be protected from possible electrostatic discharges (ESD) as well as for voltage transients originating from the electric system of the vehicle. This protection has been implemented with protection diodes compliant with the standards from Automotive Electronics Council (AEC).

3.2.3 CAN Interface

As with the voltage regulation, it is necessary to implement circuit protection for ESD that may occur on the CAN bus lines as well. In order to protect the microcontroller and circuitry associated with the CAN bus, protection diodes has been placed on the inputs of the CAN high and CAN low signal inputs. In addition to the protection diode, the CAN transceiver implemented in this design offers additional protection against voltage transients up to 8 kV.

Since the unit will be placed in an environment where signal noise will occur, the following actions has been made in order to increase the signal integrity of the CAN bus:

- Twisted Pair Cables
- Filter
- Common Mode Choke

In Figure 3.10 a schematic view of the CAN implementation can be seen complete with the filter and common mode choke.

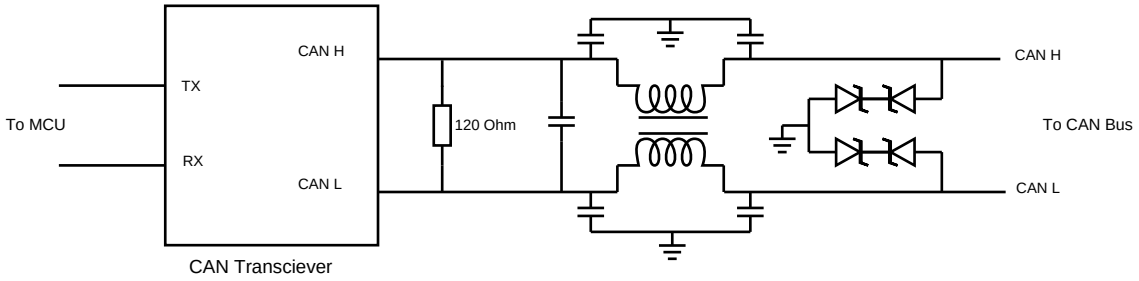

Figure 3.10: A schematic view of the CAN interface.

3.2.4 I/O Protection

In the two previous sections, the protection of the unit from common transients voltage and ESD present in the CAN bus and on the supply voltage has been discussed, but actions to protect the units more general inputs and outputs has also been taken. This was done by placing transient protection diodes on each of the digital input and output nets.

3.2.5 Enclosure

The device developed will be placed in an environment where it will become subject of sand, water and heavy vibrations. To increase the lifetime and protect the unit from this environment, the board has been designed to be compliant with an existing product enclosure developed by CPAC.

3.2.6 PCB Design

The circuit board designed has a total of 6 layers of 18 μ m thick copper. The dielectric FR-4 layers give the PCB a total thickness of 1.6 mm. The reason for choosing to design with as much as 6 layers is good EMI protection is desired in combination with 3 voltage levels for internal power supply.

In figure 3.11 the layer stack-up is shown. As can be seen 2 signal layers, 2 ground planes and 2 power layers where one is divided and used for two different

voltages. The reason behind this stack-up is that a ground plane placed close to a signal layer will help reduce the sensitivity to EMI, as well as shielding the two signal layers from each other. One power layer is dedicated to the 3,3 V power supply while the other one is divided into one part for 5 V and one part for the MCUs 1.25 V supply.

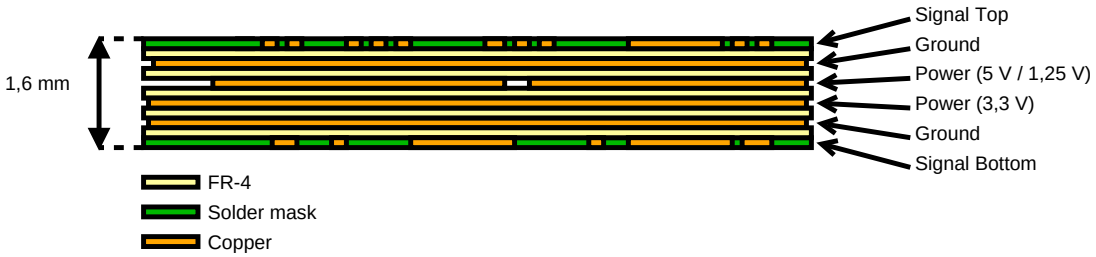

Figure 3.11: Stack-up of the controller board PCB.

3.3 Field Oriented Control

There are three distinct subsystems of the implemented control system, namely CAN communication, control loop for field oriented control and I/O. In Section 2.3.4 all necessary transformation needed for field oriented control was described, in this section we will present how field oriented control was implemented using MATLAB/Simulink. Firstly, as aforementioned, if we are to control the field of the stator by applying current, we first need to measure the current flowing in the motor. Described in following parts of this section, we use sensors based on Hall effect to measure the current flowing. In order to reduce the cost and computation time we only use two current sensors to measure the current in each phase, namely phase A and B. The last phase, in this implementation phase C is then reconstructed using Kirchhoff's law of current, as seen in Equation 3.16. In order to move to the stationary frame, the rotor position sensor also needs to be sampled to perform a correct Park transform.

$$i_a + i_b + i_c = 0 \rightarrow i_c = -(i_a + i_b) \tag{3.16}$$

Once all the currents has been transformed by Clarke and Park transformations, error signals are calculated based on the measured and demanded values for torque and new direct and quadrature values are calculated. Through inverse Park transform, new α and β values are calculated and using space vector modulation, applied to PWM modules and on to the motor.

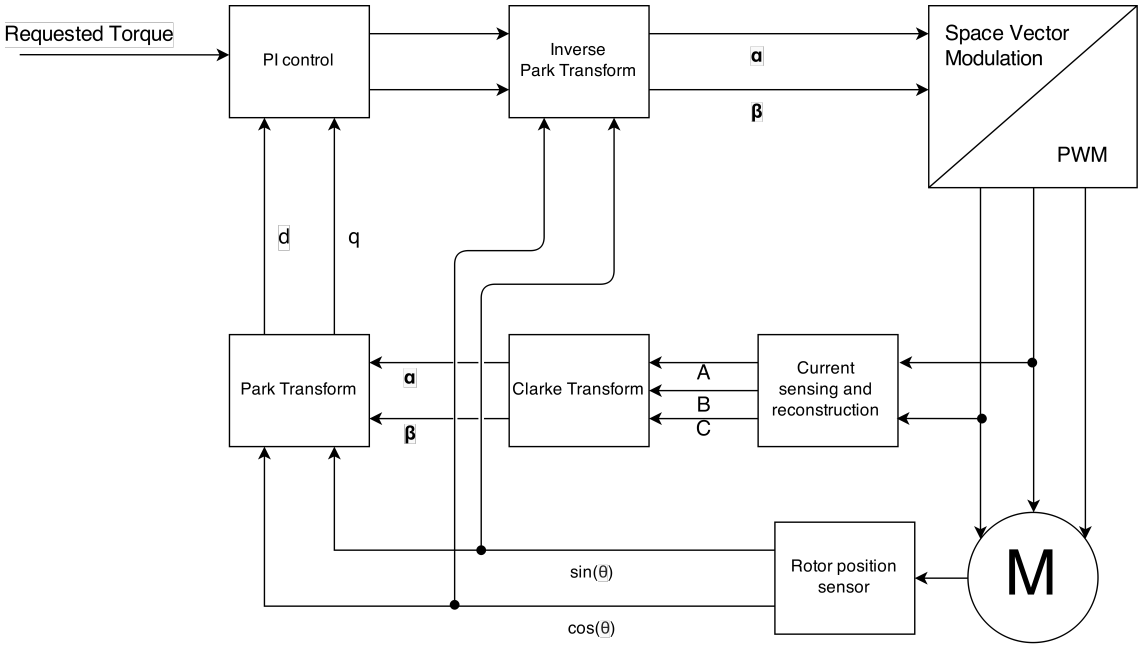

Figure 3.12: Flowchart of implementation of field oriented control.

Current Measurement

When implementing more advanced motor control algorithms such as field oriented control, a reliable and precise way of measuring the current in each phase is needed. There are two viable options to be considered when measuring current in a motor control system, one where shunt resistors are used, and the voltage drop over the shunt resistor are measured by using, preferably, a for the application specified operational amplifier called shunt monitor. The use of a shunt resistor offers an easy to use approach. The use of a single resistor offers flexibility and maintainability for the implemented hardware, should the motor specification for the motor change, in terms of current flowing through the phases, it would be easy to dimension a new shunt resistor more suitable for the new range. However, the shunt resistors need to be placed in series with the voltage source and does therefore affect the measured circuit since there is a voltage drop. The shunt resistors also dissipate a lot of power, and are not a viable solution for applications over 50 A [40].

The Hall effect sensors on the other hand offer a measurement approach that does not affect the current that are to be measured, this also means that there is no power dissipated and thus enabling the sensor to measure higher currents.

Since current only flow through each phase when the transistors in the inverter is open, it is necessary for the MCU to be able to sample the phase current regardless of the PWM pulse width. In Figure 3.13 we can see the current changes over the time the transistor is open in order to get consistency in the current sensing we would need to sample during the same interval. As also can be seen in Figure 3.13, if the currents were sampled during the middle of the time the transistor is open, we would get an

average of the current flowing in the phase. In order to be sure that every sampling of the current is done at the exact time for each new calculated duty cycle, an interrupt routine based in the PWM output was implemented. The microcontroller used in this project offer a hardware interface for this kind of interrupt routine, called Cross-Triggering Unit (CTU).

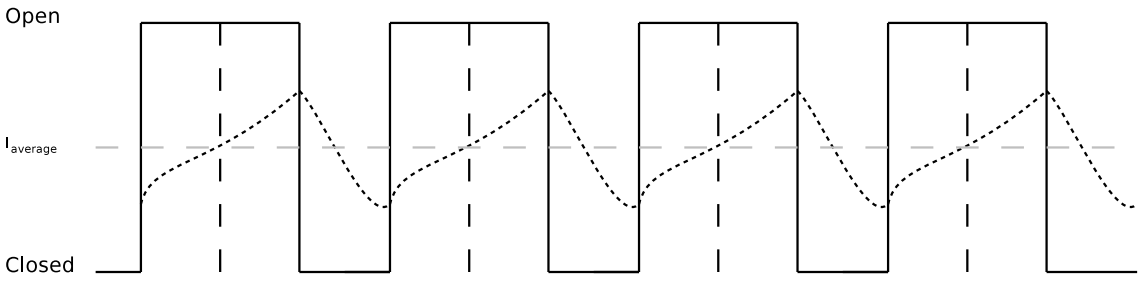

Figure 3.13: Current flowing through phases based on PWM

Rotor Position Determination

As previously mentioned, the knowledge of rotor position is a fundamental part of field oriented control. For simple control algorithms, such as the previous discussed six-step commutation, low resolution sensors, such as Hall-effect position of the rotor. There are also approaches which do not, in the sense of a pure position sensor, operate without a sensor, called sensorless. In the sensorless approach, instead the rotor position is determined by the back-emf generated by the spinning motor.

An absolute sensor was used to determine the rotor position. The rotor position encoder used in this project is of a sine/cosine type, meaning that the sensor will output two analogue signals, a sine and a cosine and comes mounted within the motor enclosure. Through trivial trigonometry the mechanical position of the rotor can be determined with a sensor accuracy of $\pm 0.5°$.

3.3.1 Motor Parameters

For this project, the motor ME1114 was available and fitted into the application specification. The motor parameters supplied by the manufacturer can be seen in table 3.2. In order to verify the torque constant and the number of pole pairs for this motor, the motor was mounted in a milling machine and rotated at a constant speed of 340 RPM. By doing this, back-EMF will be generated without commutation. The line-to-line voltages generated by this experiment can be seen in Figure 3.14. In this test the rotation encoder was enabled and in Figure 3.14 a practical example of the ratio between mechanical and electrical degrees can be seen. For this example, 4 pole pairs results in four electrical periods per mechanical period. In this figure the necessary calibration of the rotor position encoder can be seen. In this example we can see that a mechanical revolution takes 152 ms.

Table 3.2: Motor Parameters for the ME1114

ME1114	
Rated Speed	5000 RPM
Pole Pairs	4
Torque Constant	0.12 Nm/A
Armature Inertia	45 kgcm^2
Line-to-Line Inductance	0.05 mH
Line-to-Line Resistance	0.006 Ω
Peak Current	420 A

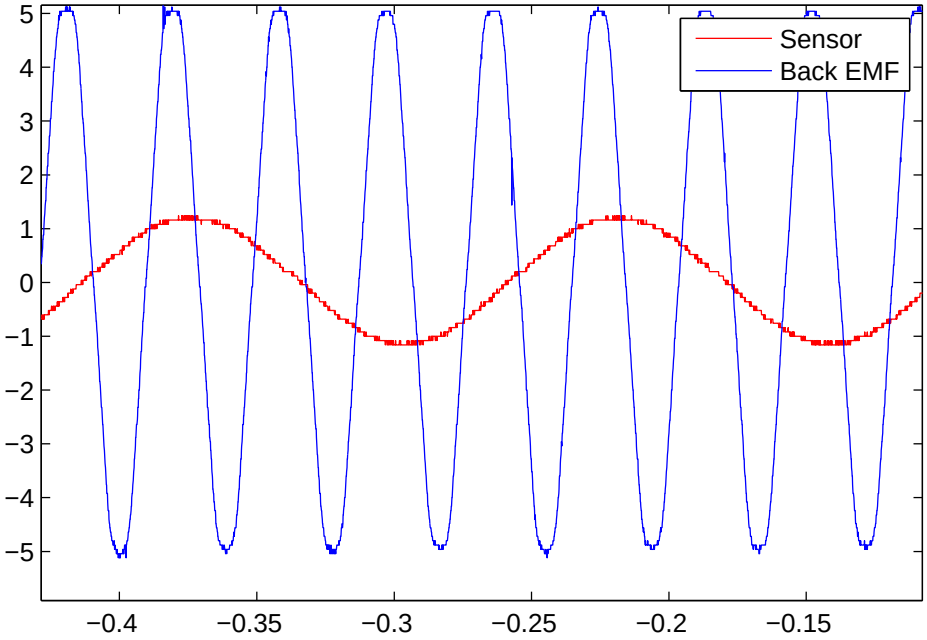

Figure 3.14: Plot showing the relations between mechanical and electrical degrees

Using this data along with the amplitude of the back-EMF measured to 5.04 V the torque constant now can be calculated as seen in Equation 3.17.

$$k_t = \frac{V_{pk}}{\omega_{el}} = \frac{5.04V}{41.34rad/s} = 0.1219 \approx 0.12 \tag{3.17}$$

3.3.2 Integrated Development Environment

Throughout this project the majority of the software is developed using Matlab/Simulink in combination with a toolbox from Freescale called Motor Control Toolbox [41]. The Motor Control Toolbox creates an integrated development environment for controlling the microcontroller implemented, and provides for software specific for the

microcontroller such as the possibility to control general purpose input and outputs, as wells as for communication peripherals such as CAN communication and SPI communication. Using a Matlab/Simulink environment for these kinds of projects moves development to a higher abstraction level, allowing for more rapid prototyping for experienced developer and offer the opportunity for otherwise unexperienced developers to implement models in a integrated system.

4 Results

An evaluation of the designed system was made to investigate several performance measures, the results from this evaluation is presented and described in this chapter. The measurement of most importance in the inverter board thermal performance, whereas the gate drive capability and overall system performance is also evaluated.

The MOSFETs used in the manufactured system is not the same as were chosen in the design phase. This was caused by problems with availability from the distributor at the time of manufacturing. Instead, a MOSFET model from the same product line was chosen with specifications according to table 4.1. The main difference between the two is that IPT015N10N5 is rated for 100 V as V_{DS} instead of 60 V as the IPT007N06N. This has effects on $R_{DS(on)}$ which will have a practical difference on the prototype manufactured. Since the $R_{DS(on)}$ of the replacement MOSFET is exactly 2 timer greater than that of the original MOSFET, a factor of 2 can conveniently be used to scale all currents in the tests.

Table 4.1: Comparison of parameters between the IPT007N06N and IPT015N10N5 MOSFETs

Parameter	IPT007N06N	IPT015N10N5	Unit
V_{DS}	60	100	V
$R_{DS(on)}$	0,75	1,5	mΩ
I_D	300	300	A
Q_{OSS}	227	213	nC
$Q_G(0V..10v)$	216	169	nC
$V_{GS(th)}(typ.)$	2.8	3.0	V

4.1 MOSFET Timings

In order to verify the correctness of the rise time calculated in 3.1.4 an oscilloscope was used to measure the rise and fall times alongside a microcontroller constantly switching the gate of a MOSFET. The findings from this test can be found in the following subsections.

4.1.1 Gate Rise Time

As discussed and calculated in Section 3.1.4 the rise time was assumed to be no longer than 200 ns for the transistors implemented. As also was mentioned, the gate driver needs to drive the MOSFETs with at least 1.06 A in order to meet this requirement. Instead of this 1.06 A the gate driver chosen will drive the transistors

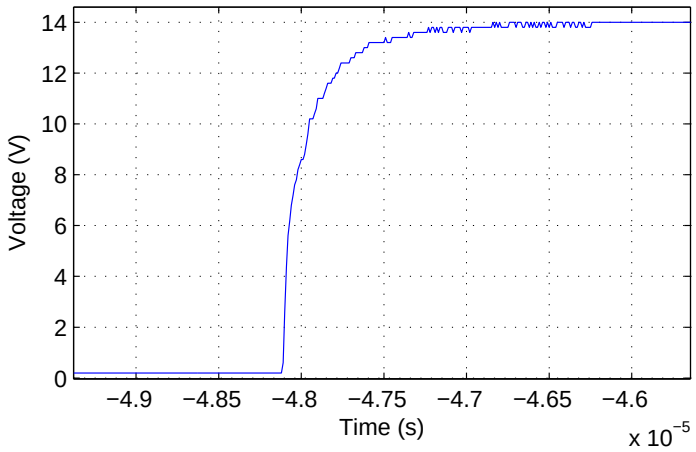

Figure 4.1: Measured rise time of gate of high side MOSFET.

with 2.11 A, which is the double amount of current. As seen in Figure 4.1 the measured rise time of the transistor to the full on 10 V is actually 160 ns and around 40 ns to the 5 V for which the transistor is able to throughput 200 A which would be higher than the actual continuous load.

The rise time of the transistor did not linearly follow the increase of driving current. This is probably since no calculations have been made regarding the increase of capacitance the oscilloscope probe will contribute with. Additionally no account for the rise-time delay of the transistors were made.

4.1.2 Gate Fall Time

The fall time of the gate is just as important as the rise time of the same gate, and a long fall time will require a software design using longer deadtimes for the PWM, or potentially damaging the circuitry. The IPT015N10N5 MOSFET has a gate threshold voltage of typically 3 V.

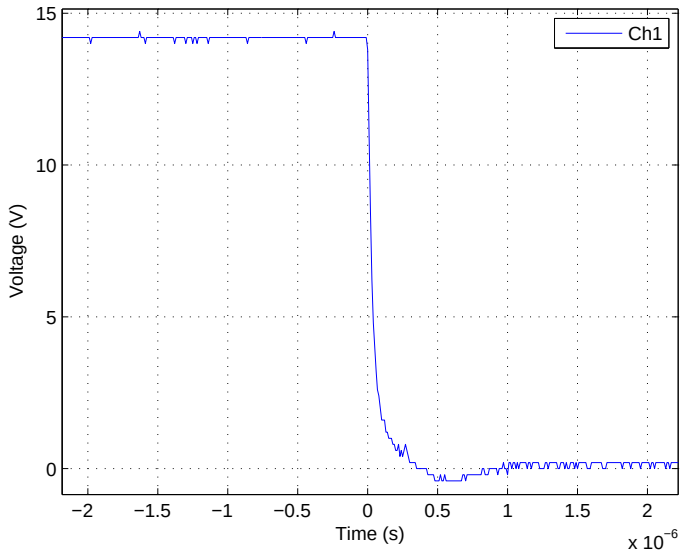

Figure 4.2: Measured fall time of gate of high side MOSFET.

As can be seen in Figure 4.2, the gate threshold voltage is reached within 80 ns which could be considered as a very fast fall time and will not pose any kinds of trouble for these kind of applications.

4.2 Thermal Analysis

A set of tests were run with a dummy inductive load in order to be able to evaluate the thermal properties of the phase-legs individually. A combination of PWM signals were applied to the gate drivers in order to enable the MOSFETs in the required manner.

The tests were conducted in a room with 18 ° C air temperature. The aluminum heat sink was placed on a large 7 mm thick steel plate with a mass of approximately 25 kg in order to simulate the thermal mass available in the real world application.

Since the tests were performed with MOSFETs that had twice the $R_{DS(on)}$ of the selected during the design phase, all currents should be up scaled with a factor of 2 in order to correspond correctly with the currents from the load profile. The

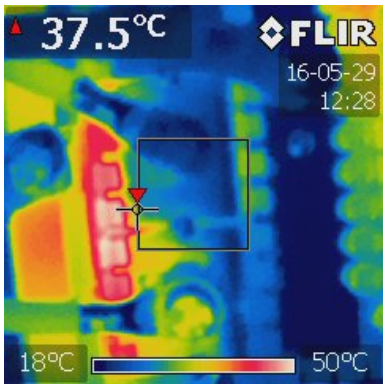

(a) Thermal measurement from test case 1.

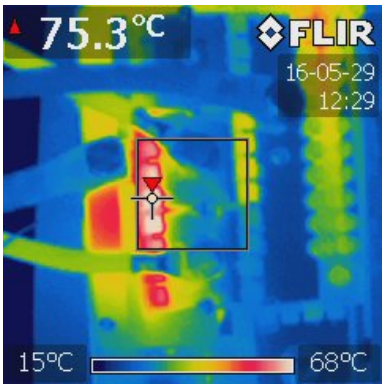

(b) Thermal measurement from test case 2.

Figure 4.3: Stable heat dissipation of inverter during low and medium high currents.

IPT015N10N5 MOSFETs that were used in the tests have a maximum allowed junction temperature of 175°C[29]. The test cases along with the results are visualized in table 4.2.

Table 4.2: Thermal result from four test cases with different load.

Test case	Current (A)	Duration (mm:ss)	MOSFET temperature (°C)
1	46	01:00	37
2	94	05:00	75
3	150	00:30	109
4	225	00:10	153

Test case 1 and 2 were performed until a stable temperature was reached. Test case 2 was ran for a more extended period since it represents a current value greater than the nominal current in the application.

Test case 3 and 4 were executed to investigate the maximum current handling abilities for short periods of time, thus simulating the peak current to the end application. These tests were halted when a too high temperature was reached.

When applying high loads to the system many observations in addition to the MOSFET temperature can be made. One of these observations is that the temperature of the electrolytic capacitors decreases with the capacitors distance from the ground terminal. Figure 4.5 shows this observation. From the same figure it is also worth to notice that the extra wide ground trace that is connecting said capacitors to ground, is heating up considerably in relation to the entirely passive area of the board. This ground trace is seen in the left part of the figure.

Another observation is the performance of the reverse input polarity protection. When voltage transients occurs due to an inductive load, the built in reverse diodes in the MOSFETs conducts the current out on the supply voltage. This is something that during our tests resulted in very high temperatures.

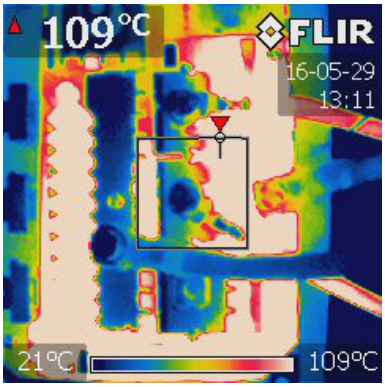

(a) Thermal measurement from test case 3.

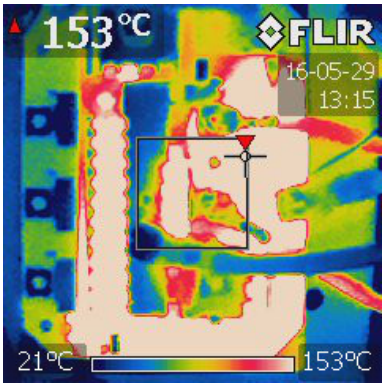

(b) Thermal measurement from test case 4.

Figure 4.4: Thermal measurements from high current test cases.

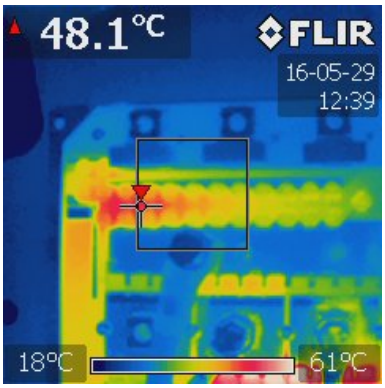

(a) Temperature measurement of electrolytic capacitors.

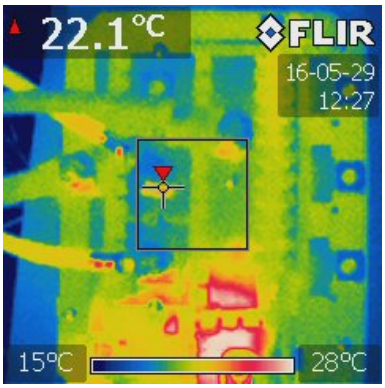

(b) Measurement of the rectifier circuit temperature.

Figure 4.5: Thermal measurements of specific components.

5 Discussion

This chapter will discuss the results presented in the previous chapter as well as possible improvements that could be done to the hardware designed in this thesis project.

The thermal evaluation shows that the driver board appears to be able to cope with the currents it was designed for. Since the tests were performed with a different MOSFET model and the current adapted to get the same power dissipation, it is not possible to be certain. To definitely determine this, additional tests would have to be performed with the originally intended MOSFETs and the full current of 400 A specified in the load profile. Other potential weaknesses such as insufficient width of the copper areas could then be revealed.

Some problems were present during the measurements of the thermal properties. Since the dummy load was inductive a voltage transient occurred at the negative terminal of the load. This made current to flow through the built in reverse diodes of the high side MOSFETs, causing additional heat to build up and disturb the thermal measurements. When considering only the MOSFETs where the current strictly passes in the forward direction, the heat built-up is lower and is well within the limits.

One discovery that was made is that in the copper area that connects the ground of the large capacitor bank with the ground terminal, heat is built up at high currents and even if the heat itself does not necessarily cause any problems, the electrical resistance of the copper area will decrease the positive effect of the capacitor bank.

One interesting finding is that even though the copper area had a temperature of 30 ° C, the power MOSFET was increasing its package temperature very rapidly, in other words, it appears that the thermal resistance between the MOSFET and the copper surface was too high, making it unable to transport the heat as fast as thought. Since the MOSFETs used are claimed to have very low thermal resistance from junction to case, this means that this problem would be hard to solve without major design changes. One possible solution could be to use MOSFETs with dual-sided cooling and heat sinks attached to both sides of the MOSFETs.

Albeit both of the designed cards fulfilled the specifications set there are some improvements that could be made. The input filter on the driver board is insufficient. Although no proper analysis has been carried out for the input filter, the input capacitance is to low for this high frequency application. This could be solved either by adding more capacitors but then a physically larger driver board needs to be developed, or by finding capacitors with higher capacitance but with the same or lower ESR. For the driver board the layer stack-up could consist, and is advised to, of more planes for signal, power and ground. The use of only two layers was

limited by the manufacturer but if multiple layers had been used it would allow for a smaller board with gate drivers closer to the MOSFETs. Using multiple layers, a central ground layer could be implemented and would allow for more capacitors, partly solving the aforementioned problem of low input capacitance.

6 Conclusion

The aim for this thesis was to create the tools needed for various control algorithms used to control a permanent magnet synchronous motor. These tools consisted of a controller board for running code, and a driver board used for inverting the DC supply voltage to a three phase AC system needed for the three phase motor.

The controller board was designed in order to guarantee future use and also to enable the use of the controller board as a general purpose electronic control unit. In order to make the controller board as future-safe as possible, it was implemented for one of the newest ASIL D certified microcontrollers and was also designed to be pin-compatible with the next-generation ASIL-D cerified microcontrollers that is to be released by Freescale Semiconductors. To add the possibility of using the controller board as a general purpose ECU, most of the peripherals was pinned out to the main connector, together with placeholders for voltage dividers and hardware filters.

The driver board was by contrast designed for this specific application. It was designed and successfully tested to be able to handle currents as high as 400 A for short durations of time and 150 A continuously.

An attempt for field-oriented control using the hardware setup was executed, but we were, due to unforeseen circumstances with the debug hardware, not able to implement the control algorithm in the hardware design. Simulations of the field-oriented control algorithm does however suggest that the application should be able to control the PMSM.

There are several possible improvements to implement on the driver board. Multiple layers would allow for smaller board with the MOSFET drivers closer to the MOSFETs. Furthermore a ground plane could be placed on a central layer, which would make it possible to add more capacitors in order to improve the stability of the motors supply voltage. There would also be no need for large areas on the board reserved to only conduct current.

Bibliography

[1] S. Anwar, *Fault Tolerant Drive By Wire Systems: Impact on Vehicle Safety and Reliability*. Dubai: Bentham Science Bentham Science Bentham Science Publishers, 2012.

[2] E. Bretz, "By-wire cars turn the corner," *Spectrum, IEEE*, vol. 38, pp. 68–73, Apr 2001.

[3] Automotive Electronics Council, "AEC documents." [Online]. Available: http://www.aecouncil.com/AECDocuments.html, Accessed May 2015.

[4] "ISO/DIS 26262-1 - Road vehicles– Functional safety – Part 1," tech. rep., Geneva, Switzerland, November 2011.

[5] "ISO/DIS 11898-1 - Road vehicles– Controller area network (CAN) – Part 1," tech. rep., Geneva, Switzerland, December 2003.

[6] L. Zhang, L. Wang, and C. Liao, "Reliability research for steer-by-wire system of electric vehicle," in *Power and Energy Engineering Conference, 2009. APPEEC 2009. Asia-Pacific*, pp. 1–4, March 2009.

[7] H. A. Toliyat, *Handbook of electric motors*, vol. 2. Marcel Dekker, 2004.

[8] A. Hughes and B. Drury, "Chapter one - electric motors and drives," in *Electric Motors and Drives (Fourth Edition)* (A. Hughes and B. Drury, eds.), pp. 1 – 38, Boston: Newnes, fourth edition ed., 2013.

[9] V. Barkhordarian, "Power MOSFET basics." International Rectifier Application Note AN-1084, Accessed May 2015.

[10] R. Locher, "Introduction to power MOSFETs and their applications." Fairchild Semiconductor Application Note AN-558, 1998.

[11] B. J. Baliga, *Fundamentals of Power Semiconductor Devices*. Springer Science & Business Media, 2010.

[12] International Rectifier, "Paralleling power MOSFETs." Application Note AN-941, Accessed May 2015.

[13] N. Hill, Christopher. Stapelberg, "Enhance MOSFET cooling with thermal vias." Power Electronics, February 2006.

[14] International Rectifier, "DirectFET technology thermal model and rating calculator." Application Note AN-1059, September 2010.

[15] Z. Shen, S. Robb, F. Robb, M. Fuchs, D. Berels, and K. Hampton, "Load dump protection in 42 v automotive electrical distribution systems," in *Applied Power Electronics Conference and Exposition, 2001. APEC 2001. Sixteenth Annual IEEE*, vol. 1, pp. 289–295 vol.1, 2001.

[16] International Rectifier, "Use gate charge to design the gate drive circuit for power MOSFETs and IGBTs." Application Note AN-944, Accessed May 2015.

[17] E. Design, "IGBTs or MOSFETs: Which is better for your design?." Electronics Design, October 1999.

[18] A. Sawle et al., "DirectFET(TM) - a proprietary new source mounted power package for board mounted power." International Rectifier White Paper, Accessed May 2015.

[19] D. Morgan, "Field-oriented control," *Embedded Systems Programming*, vol. 13, 2000.

[20] M. Barr, "Introduction to pulse width modulation (PWM)." [Online]. Available: http://www.barrgroup.com/Embedded-Systems/How-To/PWM-Pulse-Width-Modulation, November 2007.

[21] P. Madaan, "Brushless DC motors- control principles." [Online]. Available: http://www.edn.com/design/sensors/4407580/2/Brushless-DC-Motors-Part-II–Control-Principles, February 2013.

[22] Freescale Semiconductors, *Sensorless PMSM Field-Oriented Control*, April 2014.

[23] P. Satish Kumar, J. Amarnath, and S. V. L. Narasimham, "A new space-vector pulse width modulation algorithm for multilevel a new space-vector pulse width modulation algorithm for multilevel inverters," *World Journal of Modelling and Simulation*, vol. 6, no. 4, pp. 281–290, 2006.

[24] K.N. Leonard, C.M. Bingnarn, D.A. Stone and P.H. Mellor, "Implementing a sensorless brushless DC motor phase advance actuator." Texas Instruments, September 1996.

[25] Renesas Electronics, "Introduction to CAN." [Online]. Available: http://documentation.renesas.com/doc/products/mpumcu/apn/rej05b0804_m16cap.pdf, April 2006.

[26] S. Corrigan, "Introduction to the controller area network (CAN)." [Online]. Available: http://www.ti.com/lit/an/sloa101a/sloa101a.pdf, July 2008.

[27] Microchip Technology Inc, "Introduction to the controller area network (CAN)." [Online]. Available: http://www.microchip.com/stellent/groups/SiteComm_sg/documents/DeviceDoc/en558265.pdf, Accessed May 2015.

[28] Motenergy Inc., *ME1114 Datasheet*, a ed., April 2012.

[29] Infineon, *OptiMOSTMPower-Transistor, IPT015N10N5*, 2.1 ed., February 2015.

[30] Infineon, *OptiMOSTMPower-Transistor, IPT007N06N*, 2.1 ed., February 2014.

[31] Linear Technology, *LTC4357 Positive High Voltage Ideal Diode Controller*, d ed., October 2009.

[32] A. Hussain, "Driving power MOSFETs in high-current, switch mode regulators." Microchip Technology Inc. Application Note AN786, 2002.

[33] Fairchild, *FAN7190 F085 High-Current, High and Low-Side, Gate Drive IC*, October 2014.

[34] Fairchild Semiconductor, "Design and application guide of bootsrap circuit for high-voltage gate-drive ic." Application Note AN-6076, 2014.

[35] Vishay Semiconductors, *High Performance Schottky Rectifier*, July 2010.

[36] Allegro Microsystems, "Half-bridge power MOSFET controller." [Online]. Available: http://www.allegromicro.com/ /media/Files/Datasheets/A3946-Datasheet.ashx, 2013.

[37] Infineon, *TO-Leadless: A new Package for High Current High Reliability Applications*, 1 ed., May 2013.

[38] Freescale Semiconductors, *Qorivva MPC5643L Microcontroller Data Sheet*, 9 ed., June 2013.

[39] Texas Instruments, *TL5001A PULSE-WIDTH-MODULATION CONTROL CIRCUITS MANUAL*, January 1994.

[40] Analog Devices, "Measurement techniques for industrial motor control." [Online]. Available: http://www.analog.com/media/en/technical-documentation/technical-articles/Measurement-Techniques-for-Industrial-Motor-Control-MS-2652.pdf, 2014.

[41] Frescale Semiconductors, *Motor Control Development Toolbox Manual*, 2015.